Universität Bielefeld – Fakultät für Physik
Theorie der kondensierten Materie

Implementation of FTLM for full Hilbert space investigation of anisotropic quantum spin systems

Dissertation

zur Erlangung des Doktorgrades

an der Fakultät für Physik

der Universität Bielefeld

vorgelegt von

Oliver Hanebaum

am

11. Juni 2018

betreut durch

Prof. Dr. Jürgen Schnack

Abstract

Magnetic molecules promise progress in a wide variety of fields ranging from high density memory storage to quantum computing as well as magnetic cooling. In order to gain better insight this work aims at the study of theoretical models and evaluation of thermodynamic observables by implementing and testing a new numerical approximation method – the Finite-Temperature Lánczos-Method (FTLM).

Magnetic centres of molecules are modelled as spins of fixed quantum number, position and interactions. The model is specified in a spin Hamiltonian consisting of three parts: Heisenberg exchange, single ion anisotropy and Zeeman interaction. Although finite, the dimension of the Hilbert space grows exponentially with the number of spin sites, so full diagonalisation of the Hamiltonian is rendered infeasible: Even for a small number of spins the Hilbert space dimension exceeds several millions, which is beyond exact diagonalisation techniques. In order to calculate observables yet, it is necessary to implement approximation methods.

Following previous work, where the Hilbert space could be partitioned into invariant subspaces with respect to magnetic quantum numbers, now systems with anisotropy are studied. These anisotropic terms generally do not commute with total spin operators, therefore partitioning no longer helps reducing the problem size.

There are several techniques for approximate solutions to eigenvalue equations, among these adaptations of the original Lánczos method. As a Krylov subspace method, its main advantage is that the most complex operations required are matrix-vector multiplications. When matrix elements are calculated on-the-fly, the most economical version requires storage of only two vectors.

The second ingredient for FTLM is a typicality based Monte Carlo approach: Traces are estimated as an average over a tiny set of initial vectors compared to the full Hilbert space.

First tests revealed a major flaw due to numerical instability of traces that normally are zero. By partitioning with respect to magnetic quantum numbers, especially exploiting their inversion symmetry, this problem was unknowingly dodged in previous calculations. It was solved while preserving the advantage of minimal computational effort: An arbitrary set of initial vectors would regain this time-reversal symmetry only, if a substantial number of initial vectors where used. Instead, a doubling of the initial vectors by inverting them with respect to magnetic quantum numbers yields the desired effect. Time-consuming evaluations of matrix elements were also avoided by calculating the magnetisation as a difference quotient.

Finally FTLM is implemented and tested for several magnetic molecules. Analogues of the hour glass molecules synthesised by Glaser et al. were first model systems, showing good agreement of exact diagonalisation results and approximations.

The method can be applied to any Hamiltonian, given that matrix-vector products in the underlying Hilbert space can be calculated. Here limiting factors are memory usage and computing time. As a proof of principle observables in a Hilbert space consisting of $d = 100,000,000$ states were calculated using the parameter set suggested by Mazurenko et al. for the $Mn_{12}-$acetate molecule. Single crystal as well as powder averaged results are compared to experimental data. So this previously impossible calculation is now executed within hours by use of FTLM.

Acknowledgements

I am relieved and thankful, that this work is finally concluded. I owe my sincere thanks and gratitude to many people for helping me overcome obstacles on the way. Without their patience, help or advice I would not have done it. This page is dedicated to express my gratitude to all of them, even if they might not be addressed explicitly.

My special thanks go to my supervisor Jürgen Schnack, whose selfless time and motivational attitude were betimes all that kept me going. Without him even my diploma thesis would not have been possible. When I attended his statistical mechanics course he awakened my interest in theoretical physics and academic research.

Funding of the research project through the Deutsche Forschungsgemeinschaft (German Research Foundation, DFG) is gratefully acknowledged. The author gratefully acknowledges the Gauss Centre for Supercomputing e.V. for funding this project by providing computing time on the GCS Supercomputer SuperMUC at Leibniz Supercomputing Centre.

Furthermore I thank my colleagues and fellow students on E5 for stimulating and insightful discussion. Especially Jörg Ummethum is still a close friend. My supervisor and our secretary Hannelore Litschwsky became like family to me. I thank them for their moral support as well as forbearance with respect to my personal troubles. Hanne is always diligent and dedicated in giving support and advice, far exceeding her assigned job as a secretary.

My father and his mother were two strong pillars of support. Sadly both were not meant to live to see the successful conclusion of my studies. For this very reason words cannot express the gratitude and love I feel for my wife, on whose shoulders almost all the weight rested lately. I have to thank our parents for their support.

Finally I thank my wife Sonja and all friends who cheered me on, helped in many ways and shared an enjoyable time at cooking and board games as well as recreational weekend hiking tours.

Thank you all,

Oliver

Contents

List of Figures

List of Tables

Introduction

Magnetic molecules (MM) are "cool stuff with memory and use in electronics and computing". Well, molecules or particles with at least one of the aforementioned properties is what scientists are looking for. There are already MMs to be used as a coolant [1, 2]. In quantum computing [3] and spintronics – electronics with spin currents – a wide range of possible applications is expected. Another promising idea is the use of MMs as a means of memory storage [4, 5].

All these applications of MMs require different, possibly opposing, properties. In order to find an (effective) model Hamiltonian to describe MMs and predict the (non-)existence of these properties, assumptions or simplifications are made. Here molecules consisting of atoms and electrons in three-dimensional space coupled via Coulomb interaction are simplified to magnetic centres possibly in external electromagnetic fields. These are attributed a certain spin quantum number and effective intramolecular interactions such as Heisenberg or Dzyaloshinsky-Moriya as well as single-ion anisotropy accounting for their local environment. Molecules are often considered to be isolated i. e. intermolecular interactions are ignored and only an external magnetic field is applied.

The field of molecular magnetism is situated at the crossroads of thermodynamics, quantum statistics and chemical synthesis as well as computational physics. In order to model magnetic particles or molecules synthesised by chemists and predict or fit measured data it is often necessary to calculate an eigensystem of quite large, but finite-dimensional matrices. This is used to calculate the partition function and from this magnetic thermodynamic observables.

There are many different methods to calculate the partition function from a given operator. There are special cases, where analytical calculation of the full eigensystem is possible. Apart from that, numerical computations are necessary, so full or exact diagonalisation is done within a given error bound, which is either a precision goal or a machine-dependent value. For small dimensions $d < 10^5$ full diagonalisation is possible, leading to numerically exact calculations of observables. Often existing symmetries allow for separation of the underlying Hilbert space into subspaces corresponding to conserved quantities or quantum numbers, but this might reduce the relevant dimension, that is the dimension of the largest subspace, only by a small factor.

Beyond that approximations are needed, since numerical effort in terms of computing time as well as memory consumption renders exact calculations infeasible or even impossible. Even though computing power increased tremendously since the first matrix calculations on PCs, the system size grows even faster – exponentially with the number of spin centres in the magnetic quantum system.

In order to illustrate this fact consider the mythical story about the invention of chess. When asked by the local sovereign, what his reward should be, the inventor

requested a seemingly humble one: “Place one rice corn on the first field, then double the amount while traversing all sixty-four fields of the board. The sum shall be my reward.” This request was readily granted, but when the total was calculated, the tremendous number was larger than the full harvest for generations. Some versions state, that finally the inventor was executed. Others state, that this debt is a promise of alms to a certain order of monks and still collected.

To push the limit to larger systems several methods were proposed and used. The basic density matrix renormalisation group (DMRG) technique [6, 7] allows calculations of the ground state of large quantum systems, thus zero-temperature properties are accessible, extensions aim at time or temperature dependent calculations.

Other successful methods are Quantum Monte Carlo (QMC) calculations, but these suffer from the so-called sign problem, which – most fundamentally speaking – originates from the Pauli principle i. e. permutation of fermions. [7–9].

The finite-temperature Lánczos method (FTLM) discussed here originates from the Krylov subspace based Lánczos procedure for matrix (tri-)diagonalisation. The partition function is usually calculated as a trace of an operator-valued exponential function. A numerical estimate is calculated by creating Krylov subspaces using the Lánczos procedure (LP) [10, 11]. Averaging over the traces in these “local” eigensystems, which contain – in addition to the eigenvalues – weights corresponding to the overlap of local eigenstates and the initial vectors, yields approximate results. This seems to be closely related to a Riemann-Stieltjes integral formulation for the calculation of traces and matrix elements of operator-valued functions presented by Golub et al. [12–15].

FTLM calculations require a basis representation and a well defined action of a hermitian or symmetric operator on these basis states. With this approximate calculations of the partition function as well as observables for a given set of model parameters and thermodynamic variables is possible.

In Part I basic thermodynamics and the method are reviewed. After that in Part II magnetic molecules and possible terms of a spin Hamiltonian are discussed. Finally in Part III tests and results are presented.

Part I.

Finite Temperature Lánczos Method

Formica vobis exemplo sit.

–

Eighty per cent of success is showing up.
– Woody Allen

1. Lánczos Procedure

1.1. Origin and Scope

The Lánczos procedure (LP) was proposed by Cornelius Lánczos in [10, 11]. He called his improvement compared to many previous iteration methods a scheme of *minimised iterations*, which should reduce "the fatal accumulation of rounding errors". In principle the minimisation is achieved by a least-squares approach. By now there are many alternatives for matrix diagonalisation, but for high-dimensional problems it was rediscovered and many ideas for improved versions are proposed. The main reason is that only matrix-vector multiplications are necessary for iterations. Storage of sparse matrices can be applied or even calculation of matrix elements on-the-fly is possible in order to reduce memory storage consumption.

1.1.1. Krylov Subspace Methods

The basic idea of Krylov methods is the construction of a small subspace

$$\mathcal{K}_L\left(\underset{\sim}{H}, |\phi\rangle\right) = \mathrm{Span}\left(\left\{\underset{\sim}{H}^k|\phi\rangle \;\middle|\; 0 \leq k < L\right\}\right) \tag{1.1}$$

by applying the operator $\underset{\sim}{H}$ to the vector $|\phi\rangle$ repeatedly. This power method creates new vectors $\underset{\sim}{H}^k|\phi\rangle$ which are not necessarily linear independent of the $k-1$ predecessors. To find an orthonormal basis set a Gram-Schmidt procedure can be applied to the generated vectors.

The Krylov subspace dimension is at most equal to the intended number of steps L, since each step increases the subspace dimension at most by one and it stops, if a linear dependence is found. The final subspace $\mathcal{K}\left(\underset{\sim}{H}, |\phi\rangle\right)$ is called the Krylov space of $|\phi\rangle$ and the index is dropped. The Krylov space is $\underset{\sim}{H}-$invariant, which means

$$\underset{\sim}{H}|\psi\rangle \in \mathcal{K}\left(\underset{\sim}{H}, |\phi\rangle\right) \;\forall |\psi\rangle \in \mathcal{K}\left(\underset{\sim}{H}, |\phi\rangle\right) \;. \tag{1.2}$$

1.2. Recursion Relation

Construction of a basis of the Krylov subspace is a byproduct of the LP. Based on a least-squares minimisation of the overlap of the currently iterated vector $|\eta_{k+1}\rangle$ and its two predecessors $|\phi_{k-1}\rangle$ and $|\phi_k\rangle$, both an orthonormal basis as well as the matrix representation of $\underset{\sim}{H}$ with respect to it are constructed, see also Ref. [10]. Given an intermediate vector

$$|\eta_{k+1}\rangle = (\underset{\sim}{H} - \alpha_k)|\phi_k\rangle - \beta_k|\phi_{k-1}\rangle \;, \tag{1.3}$$

the parameters α_k and β_k are determined by minimising the norm of $|\eta_{k+1}\rangle$. This results in the well known three-term recursion relation

$$\beta_{k+1}|\phi_{k+1}\rangle = (\underset{\sim}{H} - \alpha_k)|\phi_k\rangle - \beta_k|\phi_{k-1}\rangle \;, \tag{1.4}$$

where

$$\beta_k = \left\langle \phi_{k-1} \middle| \underset{\sim}{H} \middle| \phi_k \right\rangle = \left\langle \phi_k \middle| \underset{\sim}{H} \middle| \phi_{k-1} \right\rangle \geq 0 \qquad \text{and} \qquad \alpha_k = \left\langle \phi_k \middle| \underset{\sim}{H} \middle| \phi_k \right\rangle \tag{1.5}$$

are matrix elements of $\underset{\sim}{H}$. The minimisation of iterations is achieved, since all iterated vectors are constructed orthogonal by this recursion. Starting from the *induction hypothesis* (IH)

$$\left\langle \phi_k \middle| \phi_{l+1} \right\rangle = 0 \quad \forall\, 0 \leq k \leq l \text{ and } \left\langle \phi_{l'} \middle| \phi_{l'} \right\rangle = 1 \quad \forall\, l' \leq l+1 \tag{1.6}$$

a proof by induction over l is done:

Base case $l = 0$:
The non-zero trial state $|\phi_0\rangle$ is orthogonal to $|\phi_{-1}\rangle = 0$.
Non-trivial base case $l = 1$:

$$\left\langle \phi_0 \middle| \phi_1 \right\rangle = \langle \phi_0 | (\underset{\sim}{H} - \alpha_0) | \phi_0 \rangle = 0 \tag{1.7}$$

$$\left\langle \phi_{-1} \middle| \phi_1 \right\rangle = 0\ . \tag{1.8}$$

Inductive step $l \to l+1$:
By construction:

$$\beta_{l+1} \left\langle \phi_l \middle| \phi_{l+1} \right\rangle = \langle \phi_l | (\underset{\sim}{H} - \alpha_l) | \phi_l \rangle - \beta_l \left\langle \phi_l \middle| \phi_{l-1} \right\rangle \qquad = 0 \tag{1.9}$$

$$\beta_{l+1} \left\langle \phi_{l-1} \middle| \phi_{l+1} \right\rangle = \langle \phi_{l-1} | (\underset{\sim}{H} - \alpha_l) | \phi_l \rangle - \beta_l \left\langle \phi_{l-1} \middle| \phi_{l-1} \right\rangle \qquad = 0 \tag{1.10}$$

Therefore consider $k < l-1$:

$$\begin{aligned} \beta_{l+1} \left\langle \phi_k \middle| \phi_{l+1} \right\rangle &= (\langle \phi_k | \underset{\sim}{H}) | \phi_l \rangle - \alpha_l \left\langle \phi_k \middle| \phi_l \right\rangle - \beta_l \left\langle \phi_k \middle| \phi_{l-1} \right\rangle \\ &= (\beta_{k+1} \langle \phi_{k+1}| + \alpha_k \langle \phi_k| + \beta_k \langle \phi_{k-1}|) | \phi_l \rangle \\ &\quad - \alpha_l \left\langle \phi_k \middle| \phi_l \right\rangle - \beta_l \left\langle \phi_k \middle| \phi_{l-1} \right\rangle \\ &= 0\ , \end{aligned} \tag{1.11}$$

by (IH) since $k < l-1$.

Theoretically this property ensures that iterating yields new trial vectors orthogonal to all preceding ones. Thus iterations do not enter already explored directions and the number of iterations is reduced.

1.3. Algorithmic Description of LP

1.3.1. Properties in Exact Arithmetics

First we consider the best of worlds, where computing power and storage are limitless: Calculations are executed instantaneously with infinite precision and all iterated vectors are stored. As a result no rounding errors or numerical instabilities occur.

Iteration by the recursion relation yields an orthonormal basis

$$\{|\phi_k\rangle\}_{k=0,..,L-1} \text{ with } |\phi_0\rangle = |\phi\rangle \text{ of } \mathcal{K}_L\left(\underset{\sim}{H}, |\phi\rangle\right) . \tag{1.12}$$

Furthermore, the matrix representation of $\underset{\sim}{H}$ with respect to this basis set is a tridiagonal symmetric matrix T_L where the α's appear on the main diagonal and the β's, starting from $k = 1$, appear on the first upper and lower diagonals. Assume that a finite set $\{\lambda_k \mid k = 0, .., P-1\}$ of pairwise different eigenvalues or – a little more specific – linear combinations of corresponding eigenstates, participate in the initial state. Then after exactly $P-1$ steps the iteration stops with $|\phi_P\rangle = 0$.

The approximate eigensystem of T_P

$$\{(\mathcal{E}_l, |\psi_l\rangle) : T_P|\psi_l\rangle = \mathcal{E}_l|\psi_l\rangle , l = 0, .., P-1\} \tag{1.13}$$

is in fact an exact eigensystem of $\underset{\sim}{H}$, restricted to the unique Krylov subspace

$$\mathcal{K}\left(\underset{\sim}{H}, |\phi\rangle\right) = \mathcal{K}_P\left(\underset{\sim}{H}, |\phi\rangle\right) , \tag{1.14}$$

while the approximate eigenvalues coincide with the participating eigenvalues.

1.3.2. Standard Algorithm

Algorithm 1.3.1 (Standard Lánczos Algorithm)
Initialise: $k = 1$, $|\phi_{-1}\rangle = 0$, *random* $|\phi_0\rangle$, *tolerance* $\varepsilon = 10^{-8}$.

1. *Compute* $|\phi'_k\rangle = \underset{\sim}{H}|\phi_{k-1}\rangle$.
2. *Compute* $\alpha_k = \left\langle \phi_{k-1} \middle| \phi'_k \right\rangle$, $\beta_k = \left\langle \phi_{k-2} \middle| \phi'_k \right\rangle$
3. *Compute* $|\phi''_k\rangle = |\phi'_k\rangle - \alpha_k|\phi_{k-1}\rangle - \beta_k|\phi_{k-2}\rangle$
4. *Calculate* $\eta'_k = \sqrt{\left\langle \phi''_k \middle| \phi''_k \right\rangle}$
5. *If* $\eta'_k > \varepsilon$ *set* $\eta_k = {\eta'_k}^{-1}$, *else* $\eta_k = 0$.
6. *With this calculate next vector* $|\phi_k\rangle = \eta_k|\phi''_k\rangle$.
7. *Check termination criteria:*
   - *Non-zero norm of new vector:* $\eta_k > 0$
   - *Convergence of ground state* $\left|\mathcal{E}_0^{(k)} - \mathcal{E}_0^{(k-1)}\right| < \varepsilon$
   - *Maximum number of iterations reached:* $N_L = k$
   - *Test of further conditions*
8. *If no termination, increase* k *and continue with step two.*

This standard algorithm (1.3.1) usually requires storage of three vectors in order to perform iterations. Opposed to exact arithmetics there are limitations to bear

in mind: Each number stored and processed in floating-point arithmetics is only a representation of the true value within a machine-specific error bound f. Investigation of error estimates and algorithmic error propagation are part of Numerical Mathematics. Since finding rigorous estimates is not within the scope of this thesis, merely qualitative observations will be discussed.

So what happens qualitatively, when the assumptions of infinite precision and computing power are dropped? Rounding errors occur that subsequently accumulate. The iterated vectors lose the long distance orthogonality, when the first eigenvalue, usually the one with largest absolute value, converges. Due to accumulated errors, there are still components of the corresponding eigenstate participating in the next iterated vectors. These are inflated in the normalisation step and more so in the multiplication step, where each eigenstate in the linear combination representing the iterate is effectively multiplied by the corresponding eigenvalue. Thus ghost copies of converged eigenvalues emerge and orthogonality is lost. Fortunately these ghosts do not have a significant weight, so there is a less disruptive influence than might be expected.

However, one notable fact is that approximate eigenvalues repeated over successive iterations correspond to true eigenvalues, whereas most of the approximate eigenvalues are more or less equidistant and move with each iteration. Their positions correspond to the zeros of an orthogonal sequence of polynomials – the characteristic polynomials of the tridiagonal matrices constructed throughout the Lánczos iterations. As a result of this process zeros of one polynomial are separated by those of the preceding one. Furthermore all zeros have a multiplicity of one and successive polynomials do not share zeroes, at least in infinite precision. So one could argue that the emergence of higher multiplicity indicates a breakdown of orthogonality and thus is a hard termination condition.

In the pantaeder test case (Chapter 5), where eigenvalues are well separated, early termination – with respect to the numbers of iterations – often occurred. This happened when all eigenvalues were found. This does not guarantee good agreement with true eigenvalues. Those not present in earlier iterations, especially the last one, exhibit errors in the per cent range.

Concerning termination criteria there are several further options. The most obvious are termination by ground state convergence as well as reaching a significant error measure. Further equations, that hold in infinite precision, could be used for fine-tuning conditions to abort if the deviation of iterates from these exceeds a given tolerance.

1.3.3. Two-vector Algorithm

Step three in the two-vector algorithm (1.3.2) is not really an increase in complexity: Since matrix elements are calculated on-the-fly, a custom routine for matrix-vector multiplication is necessary. When calculating $|\psi\rangle$ component-by-component there is only a small step to calculating α's simultaneously. This two-vector version might not improve in terms of numerical errors, but it reduces the required memory by nearly one third. This allows to perform LP for the Mn_{12} – acetate molecule synthesised by Lis [16] with complex-valued vectors in a vector space of dimension

Algorithm 1.3.2 (Two-vector Algorithm)
Initialise $|\psi\rangle = 0$, *random* $|\phi\rangle \neq 0$, $\varepsilon > 0$.

1. $\beta_k = \left\langle \phi \middle| \phi \right\rangle$, $\gamma_k = \beta_k^{-\frac{1}{2}}$. *If* $\beta_k < \varepsilon$ *set* $\eta_k = 0$.
2. $|\phi\rangle = \gamma_k |\phi\rangle$, $|\psi\rangle = -\gamma_k^{-1} |\psi\rangle$
3. *Calculate simultaneously*
$$|\psi\rangle = |\psi\rangle + \underset{\sim}{H}|\phi\rangle \quad \textit{and} \quad \alpha_k = \left\langle \phi \middle| \underset{\sim}{H} \middle| \phi \right\rangle = \left\langle \phi \middle| \psi \right\rangle$$
4. $|\psi\rangle = |\psi\rangle - \alpha_k |\phi\rangle$
5. *Exchange references* $|\phi\rangle \leftrightarrow |\psi\rangle$

   Increase k *and repeat while:*

   - $\beta_{k-1} > \varepsilon$
   - $k <= N_L$ = *max iterations*
   - *Test of further (fine-tuning) conditions*

$d = 100,000,000$ on a standard desktop PC [1]. The possibility of a two-vector version is mentioned by C. C. Paige [17].

1.4. Development and Analysis of LP

Although theoretically the basic LP should work smoothly, one intrinsic problem was encountered: At some point the method breaks down due to a "loss of orthogonality". This happens either due to numerical instability, or convergence of extremal eigenvalues and emergence of ghost copies. This is addressed in Refs. [18, 19] as well as application of LP in matrix diagonalisation, numerical stability and error estimates.

Much effort has been made to overcome this obstacle and different improved methods were developed. Normally, also in my diploma thesis, full reorthogonalisation (FRO) was used to improve results of LP. Thus, at least for small ($d \lesssim 10^5$) matrices, the possible number of steps until breakdown is increased and better convergence of eigenvalues is observed. According to Simon [20] FRO is inefficient compared to partial reorthogonalisation, since "the extra orthogonality gained does not produce a more accurate" tridiagonal matrix.

The block LP [21, 22] takes a set of orthogonal starting vectors and iterates this set. As a result, multiple eigenvalues are calculated and their algebraic multiplicities can be resolved better.

A different approach is a restarted LP [23, 24], where the accumulation of rounding

[1] Referring to the 32-bit memory barrier of about 3 GB.

errors and the resulting non-orthogonality is monitored. After reaching a given error threshold LP is restarted with the last iterate as starting vector while keeping already converged eigenvectors.

1.4.1. Rayleigh Quotient and Ritz Values

For a given (hermitian) operator $\underset{\sim}{H}$ operating in a $d-$dimensional Hilbert $\mathcal{H}$ space and any non-zero vector $|\phi\rangle \in \mathcal{H}$ the Rayleigh quotient is defined as

$$R(\phi) = \frac{\left\langle \phi \middle| \underset{\sim}{H} \middle| \phi \right\rangle}{\left\langle \phi \middle| \phi \right\rangle} . \tag{1.15}$$

Assuming that the eigenvalues $\{\lambda_k\}_{k=1\ldots d}$ of $\underset{\sim}{H}$ are in ascending order, it is true that

$$\lambda_1 \leq R(\phi) \leq \lambda_d \; \forall |\phi\rangle \in \mathcal{H} . \tag{1.16}$$

If the Krylov subspace of a given vector $|\phi\rangle$ is found, the (orthogonal) complement is also an invariant subspace of $\mathcal{H}$ and the eigenvalue problem is reduced to two smaller problems. For LP this means that the constructed tridiagonal matrix is the representation of $\underset{\sim}{H}$ in the Krylov subspace and its eigenvalues are eigenvalues of $\underset{\sim}{H}$.

Diagonalising tridiagonal matrices from intermediate steps of LP only yields approximate sets of eigenvalues and eigenvectors $\left\{ \left(\theta_k^{(L)}, \left| \psi_k^{(L)} \right\rangle \right) \right\}_{k=0,\ldots,L-1}$, often referred to as Ritz values and Ritz vectors. For these the residual norm squared is known [18, 19] to be

$$\left\langle \psi_k^{(L)} \middle| \left(\underset{\sim}{H} - \theta_k^{(L)} \underset{\sim}{\mathbb{1}} \right)^2 \middle| \psi_k^{(L)} \right\rangle = \beta_L^2 \left| \left\langle \phi_L^{(L)} \middle| \psi_k^{(L)} \right\rangle \right|^2 . \tag{1.17}$$

According to Krylov and Bogoliubov [2] this leads to an eigenvalue inclusion principle. As a result for each k there exists an eigenvalue λ of $\underset{\sim}{H}$ with

$$\left| \lambda - \theta_k^{(L)} \right| \leq \beta_L \left| \left\langle \phi_L^{(L)} \middle| \psi_k^{(L)} \right\rangle \right| . \tag{1.18}$$

The scalar product $\left\langle \phi_L^{(L)} \middle| \psi_k^{(L)} \right\rangle$ is the last component of the k-th eigenvector of the L-dimensional tridiagonal Lanczos matrix. So this could be used to measure convergence of eigenvalues.

[2] Original reference unavailable. Maybe Russian or French, approximately 1930. Found in slides9 at http://people.inf.ethz.ch/arbenz/ewp/slides.html.

2. Finite-temperature Part of FTLM

2.1. Partition Function and Observables

Evaluation of thermodynamic observables is based on statistical mechanics found in standard textbooks [25–27].

The models investigated here are finite quantum systems, where mechanical properties, i. e. influence of the molecules structure, pressure or strain, are ignored. These determine model parameters, but are otherwise taken to be constant, so observables are only influenced by temperature T and external magnetic field $\vec{B}$. A system is modelled by a spin Hamiltonian operating on states in a finite-dimensional Hilbert space. The partition function and thermodynamic expectation values $\langle\langle\ \cdot\ \rangle\rangle$ of given operators $\underset{\sim}{Q}$ are evaluated as traces of these operators multiplied by the statistical operator $\underset{\sim}{\rho}_c$ of the canonical ensemble:

$$\underset{\sim}{\rho}_c = \exp\left(-\beta \underset{\sim}{H}\right)\ ,\ \beta^{-1} = k_B T \tag{2.1}$$

$$Z = \langle\langle\ \underset{\sim}{\mathbb{1}}\ \rangle\rangle = \mathrm{Tr}\left[\underset{\sim}{\rho}_c \underset{\sim}{\mathbb{1}}\right] = \mathrm{Tr}[\exp\left(-\beta \underset{\sim}{H}\right)] \tag{2.2}$$

$$\langle\langle\ \underset{\sim}{Q}\ \rangle\rangle = \frac{1}{Z}\mathrm{Tr}[\underset{\sim}{Q}\exp\left(-\beta \underset{\sim}{H}\right)]\ . \tag{2.3}$$

Considering T and $\vec{B}$ as external parameters leads to defining a thermodynamic potential

$$G\left(T, \vec{B}\right) = -\frac{1}{\beta}\ln\left(Z\left(T, \vec{B}\right)\right)\ , \tag{2.4}$$

which has just these as variables. With this relevant observables – such as magnetisation $\vec{M}\left(T, \vec{B}\right)$, magnetic susceptibility $\overset{\leftrightarrow}{\chi}\left(T, \vec{B}\right)$ or heat capacity $C\left(T, \vec{B}\right)$ – are obtained as first or second derivatives of $G\left(T, \vec{B}\right)$:

$$\vec{M}\left(T, \vec{B}\right) = -\frac{\partial G\left(T, \vec{B}\right)}{\partial \vec{B}} \tag{2.5}$$

$$C\left(T, \vec{B}\right) = \frac{\partial G\left(T, \vec{B}\right)}{\partial T} \tag{2.6}$$

$$\overset{\leftrightarrow}{\chi}\left(T, \vec{B}\right) = \frac{\partial \vec{M}}{\partial \vec{B}} = \left(\frac{\partial M_k}{\partial B_l}\right)_{k=x,y,z;\, l=x,y,z} \tag{2.7}$$

From now on the external field's direction $\vec{e}_B$ is fixed and taken as z-direction and only scalar functions of B are considered:

$$M\left(T,B\right) = -\frac{\partial G\left(T,B\right)}{\partial B} \tag{2.8}$$

$$\chi\left(T,B\right) = \frac{\partial M}{\partial B}\,. \tag{2.9}$$

For large temperature a Curie law

$$\chi\left(T,B\right) = \frac{K_J}{T}\;,\; K_J = \frac{g_J^2 \mu_{\mathrm{B}}^2 J(J+1)}{3k_{\mathrm{B}}} \tag{2.10}$$

is expected, where $J = L+S$ denotes the total of spin and orbital angular momentum and

$$g_J = \frac{3}{2} + \frac{S(S+1) - L(L+1)}{2J(J+1)} \overset{L=0}{=} 2\,. \tag{2.11}$$

Since only transition metal ions with quenched orbital angular momentum are relevant here, we almost always have $g_J \approx 2$.

So as an alternative to $T\,\chi$ or χ^{-1} in order to fit model parameters to experimental data another interesting observable is the effective magnetic moment

$$\mu_{\text{eff.}}\left(T,B\right) = \sqrt{3k_B T\,\chi\left(T,B\right)}\,. \tag{2.12}$$

In experimental data χ is approximated as M divided by B:

$$\mu_{\text{eff.}}\left(T,B\right) \approx \sqrt{3k_B \frac{T}{B}\,M\left(T,B\right)}\,. \tag{2.13}$$

In terms of dimensionless quantities, where $\mathrm{M}\left(T,B\right)$ and $\mu_{\text{eff.}}\;\left(T,B\right)$ are measured in units of μ_{B}, T in kelvin and B in tesla, we have

$$\left(\frac{\mu_{\text{eff.}}\left(T,B\right)}{\mu_{\mathrm{B}}}\right) \approx 2.57861 \times \sqrt{\left(\frac{T}{1\,\mathrm{K}}\right)\left(\frac{1\,\mathrm{T}}{B}\right)\left(\frac{\mathrm{M}\left(T,B\right)}{\mu_{\mathrm{B}}}\right)}\,. \tag{2.14}$$

At high temperatures interactions are less relevant and spins act like a paramagnet. That is why the high temperature limit of $\mu_{\text{eff.}}$ is called paramagnetic limit. Its value is

$$\mu_{para.}^2 = \mu_{\mathrm{B}}^2 \sum_k g_{s_k}^2 s_k(s_k+1)\,. \tag{2.15}$$

2.2. Use of Difference Quotients

In general, thermodynamic observables are evaluated as traces of operators weighted by the statistical operator.

Computational effort for matrix transformations scales asymptotically as d^3 where d is the relevant dimension. FTLM scales linearly in d, which is less complex. So if an approximate differential (two-sided differential quotient) is used, the actual

effort of FTLM is only doubled, so that evaluation of observables does not lead to an intense increase in computational effort. For $\Delta B > 0$ the magnetisation is equal to the directional derivative along $\vec{e}_B$:

$$M(T,B) \approx \frac{-1}{2\Delta B}(G(T,(B+\Delta B)\vec{e}_B) - G(T,(B-\Delta B)\vec{e}_B)) \,. \tag{2.16}$$

For calculation of the effective magnetic moment the magnetic susceptibility is replaced by the quotient of M and B, as it is often done with experimental data. Thus second derivatives of G are avoided and it is possible to calculate all observables by evaluating traces of functions $\mathrm{f}(\underset{\sim}{H})$ only.

2.3. FTLM Approximations

The main idea of FTLM is to replace traces of operators by random sampling of R vectors $|r\rangle$ and averaging the expectation values with respect to these samples [28]:

$$Z = \mathrm{Tr}[\exp(-\beta\underset{\sim}{H})] \approx \frac{\mathrm{Dim}(\mathcal{H})}{R}\sum_{r=1}^{R}\langle r|\exp(-\beta\underset{\sim}{H})|r\rangle \tag{2.17}$$

$$\langle\langle\ \underset{\sim}{O}\ \rangle\rangle = \frac{1}{Z}\mathrm{Tr}[\underset{\sim}{O}\exp(-\beta\underset{\sim}{H})] \approx \frac{\mathrm{Dim}(\mathcal{H})}{R}\sum_{r=1}^{R}\langle r|\underset{\sim}{O}\exp(-\beta\underset{\sim}{H})|r\rangle \tag{2.18}$$

Functions f of operators are usually calculated via a series expansion of $\mathrm{f}(x)$ and by using a spectral representation of the operator. So the main missing ingredient is the approximate spectral decomposition of $\underset{\sim}{H}$. This is where LP is used: By applying LP for $\underset{\sim}{H}$ and each sample state $|r\rangle$ the Krylov subspaces

$$\mathcal{K}_{N_L}(\underset{\sim}{H},|r\rangle)\ \ , r = 1,2,...,R$$

are obtained as well as approximate spectral decompositions

$$\underset{\sim}{H} \approx \sum_{l=1}^{N_L}\left|\psi_l^{(r)}\right\rangle\mathcal{E}_l\left\langle\psi_l^{(r)}\right| \,, \tag{2.19}$$

where the $\mathcal{E}_l^{(r)}$ and $\left|\psi_l^{(r)}\right\rangle$ are eigenvalues and eigenvectors of the tridiagonal matrix representation of $\underset{\sim}{H}$ in the respective subspaces. With this approximate spectral decompositions of functions of $\underset{\sim}{H}$ and traces are calculated as

$$\mathrm{f}(\underset{\sim}{H}) \approx \sum_{l=1}^{N_L}\left|\psi_l^{(r)}\right\rangle f\left(\mathcal{E}_l^{(r)}\right)\left\langle\psi_l^{(r)}\right| \tag{2.20}$$

$$\mathrm{Tr}[\mathrm{f}(\underset{\sim}{H})] \approx \frac{\mathrm{Dim}(\mathcal{H})}{R}\sum_{r=1}^{R}\sum_{l=1}^{N_L}\left|\left\langle r\middle|\psi_l^{(r)}\right\rangle\right|^2 f\left(\mathcal{E}_l^{(r)}\right) \,. \tag{2.21}$$

These approximate calculations are similar to the Riemann-Stieltjes integral approach in Refs. [13, 15].

2.4. Powder Averaging

Samples of magnetic molecules are in general crystals or a powder of these. In order to model a powder sample, it is assumed that the magnetic molecules or small crystals are oriented randomly in space. Thus measurement of magnetic properties in powder samples averages over all possible orientations relative to the magnetic field direction. This behaviour is mimicked by calculating observables for directions given by Lebedev-Laikov grids [29] or similar sets of directions.

dir	x	y	z
A	0.57735	0.57735	0.57735
B	-0.57735	0.57735	0.57735
C	0.57735	-0.57735	0.57735
D	0.57735	0.57735	-0.57735
E	0.	0.35682	0.93417
F	0.	-0.35682	0.93417
G	0.93417	0.	0.35682
H	-0.93417	0.	0.35682
I	0.35682	0.93417	0.
J	-0.35682	0.93417	0.

Table 2.1.: Directions used in powder averaging
These ten directions are the corners of a dodecahedron in one hemisphere and have equal weight for powder averaging.

The idea is, that any integral over the unit sphere is approximated by a weighted sum over the set $\mathcal{P}$ (as in Table 2.1) of these points:

$$\int_0^{2\pi}\int_0^{\pi} \mathrm{f}(\theta,\varphi)\sin(\theta)\,\mathrm{d}\theta\mathrm{d}\varphi \approx 4\pi \sum_{\vec{x}\in\mathcal{P}} \mathrm{f}(\vec{x})\ \mathrm{w}(\vec{x})\ . \tag{2.22}$$

One question arose, concerning calculation of thermodynamic quantities as derivatives of the partition function or a thermodynamic potential: *Which order is correct: First calculate the average, then differentiate – or in reverse order?*

Considering the experimental setup one could argue, that the measurement taken is a superposition of different contributions originating from randomly oriented crystals in a powder sample.

At least for magnetisation and $\mu_{\text{eff.}}$ it is easy to decide which way is correct. Since we know that a superposition principle exists for magnetisation and fields, calculating $\mu_{\text{eff.}}$ from a magnetisation average is the natural way.

2.5. Implementation of Magnetisation "Measurement"

Depending on standpoint, there are two different ways to implement measurement of the magnetisation component parallel to the field direction: Either do not change

the system, calculate $\underset{\sim}{\vec{M}}$ and project onto $\vec{e}_B$, or rotate the system (parameters) such that $\vec{e}_B$ becomes the z-direction and calculate M_z. My choice was the second version, since less multiplications of full-dimensional (though sparse) matrices and vectors are required, especially for evaluation of M. The parameter transformations are done as product of five complex-valued three-dimensional matrices. This yields an analytically precalculated matrix with only two rotation angles as transformation parameters.

Often experiments involve time-dependent fields and other external parameters. This aspect of experimental setup is not taken into account, instead it is assumed that systems are in thermodynamic equilibrium during measurement.

Part II.

Molecular Magnetism

Repetitio est mater studiorum.

–

3. Overview and Motivation

3.1. Motivation

Now let us leap forward to the relatively new field of molecular magnetism (MM). As a rough first definition MM is an interdisciplinary area of research connected to low temperature physics and several branches of chemistry such as synthesis and theory. But first of all magnetism emerged as a subject in solid state physics and materials science, since ordinary magnets are solids that exhibit a permanent magnetic field at room temperature. So how can a molecule be a magnet? At least below a certain temperature, a magnet has a non-zero magnetic moment. Or, more carefully, magnetisation data of magnetic molecules exhibits a hysteresis loop under periodic variation of the external magnetic field around zero [30].

There are several target areas of application with specific required properties. In almost all cases it helps to have a well separated low lying multiplet such that the effective Hamiltonian has a simple structure, good quantum numbers and without mixing perturbation. For quantum computing or information storage this usually means cooling with liquid helium to very low temperatures.

Magnetic cooling

Almost any magnetic material is a possible coolant due to the magnetocaloric effect (MCE). This effect is enhanced near phase transition like magnetisation steps, where small differences in magnetic field correspond to high entropy differences. For MCE-based cooling an efficiency above sixty per cent of the Carnot efficiency is predicted, which is better than the forty per cent reached by the prevalent vapour compression technology. "Along with the prospect of higher efficiency, magnetic cooling offers a lower environmental impact, as no hazardous fluids and only a few movable parts (low noise pollution) are used" [31].

Quantum computing

Prerequisites for quantum computing seem contradictory: On the one hand you need an isolated system, ideally without external influence, in order to avoid decoherence. On the other hand easy access is required in order to manipulate the system and extract results. DiVincenzo's requirements for quantum computing [32] are discussed in a tutorial review on *Design of magnetic coordination complexes for quantum computing* [33]: In order to have well characterized qubits in magnetic molecules one needs either a system with a $S = \frac{1}{2}$ ground state or a bi-stable system with a well separated ground state doublet. They say, that scalability is easily achieved by chemical methods. The initialisation would be done by applying a magnetic field and cooling down. "For spin-based qubits decoherence can mainly arise through

interaction with phonons and nuclear spins, as well as dipolar interactions with neighbouring qubits. In this respect, the necessary coupling between qubits during computation may be in itself a source of decoherence" [33]. A "universal" set of quantum gates, where quantum gate means applying an unitary transformation to two qubits. This corresponds to a time evolution with a simple Hamiltonian, which ideally couples only the low-lying qubit-states. In order to carry out these two operations it is necessary that the qubits of the QG have the possibility to exhibit entangled states.

"The state of the target qubits within the quantum gates, i. e. the output, has to be determined once the computation is finished. This implies that any qubit, including those within QGs, has to be addressed selectively, either spatially, spectrally, magnetically or by any other means. It is clear from above that implementing QC using coordination chemistry is a very difficult prospect, and a huge synthetic challenge" [33].

Information storage

For information storage it is necessary to have long-lived states to represent bits or qubits. One idea is to use a system with bi-stable ground state with high anisotropy barrier in order to prevent magnetisation tunnelling. Usually magnetic systems with zero-field splitting ($D < 0$) are considered. Without external field states with minimal energy are arbitrary linear combinations of the states with extremal magnetic quantum number $\pm S$.

Quite recently single-atom magnets were successfully used in an experimental data storage device [34]. Isolated Holmium atoms adsorbed on magnesium oxide were manipulated using a scanning tunnelling microscope (STM). The magnetic state was switched by applying a pulsed tunnel current and read out through the tunnel magnetoresistance.

"The catch with SMMs is their memory effect works only under the influence of a magnetic field at very low temperatures, up to 14 K so far, using liquid helium as a coolant. The new dysprosium molecule displays magnetic switchability up to 60 K" [35, 36].

$Mn_{12}-$acetate

One famous molecule in this field is the $Mn_{12}-$acetate, which essentially, in terms of magnetic ions or sites, consists of twelve manganese ions. A spin quantum number of $s = \frac{3}{2}$ is attributed to four of these, the remaining eight have a spin of $s = 2$. Therefore the spin Hilbert space has dimension $d = 100,000,000$, which is at the moment far beyond full diagonalisation techniques. In the ground state the spins of equal quantum numbers are aligned parallel to each other and spins of different quantum numbers are aligned antiparallel, so that the resulting total (GS) spin is $S = 10$.

Figure 3.1 shows high field magnetisation data calculated for different Heisenberg only parameter sets. One common feature is the high stability of the $S = 10$ ground state. At least $B = 90\,\mathrm{T}$ are necessary to reach higher values of S. Measurement

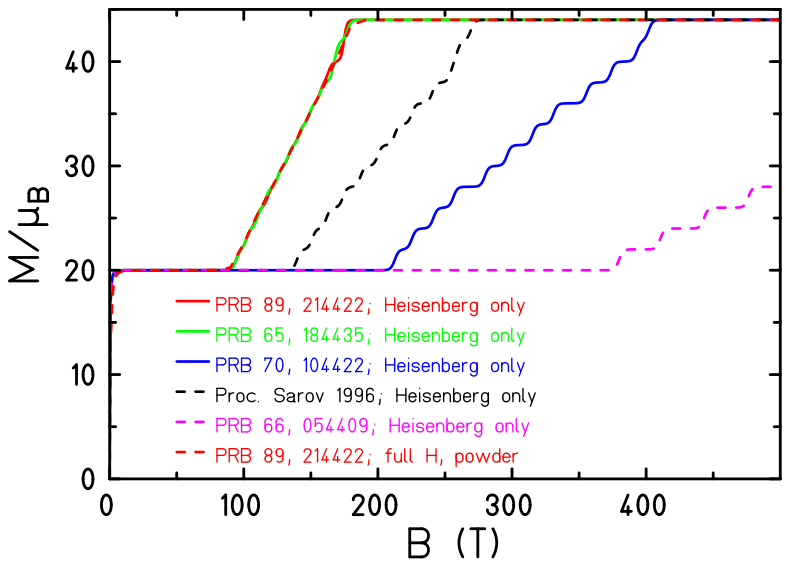

Figure 3.1.: High field magnetisation calculated for $Mn_{12}-$acetate
High field magnetisation calculated for $Mn_{12}-$acetate at $T = 2\,\mathrm{K}$ [37]

at such extreme values of magnetic field are hard or even impossible today. [1] Nevertheless measurement of the magnetisation (steps) would easily rule out several proposed parameter sets.

[1] REMARK: (2015) Highest non-destructive magnetic field at about 100 T for 15 ms in a pulsed magnet; https://nationalmaglab.org

4. Spin Systems

Some basic facts concerning spin systems are presented here. Mainly the Hamiltonian is introduced and possible terms are discussed. The special case of spin triangles or more generally *pantaeders*[1] is discussed later as a test case in Chapter 5.

4.1. Basics

Here The eigenvalue equations of spin operators are

$$\underset{\sim}{S}^z|s,m\rangle = \hbar m|s,m\rangle \tag{4.1}$$

$$\vec{\underset{\sim}{S}}^{\,2}\,|s,m\rangle = \hbar^2 s(s+1)|s,m\rangle, \tag{4.2}$$

where s may take integer or half-integer values, while m takes values with integer distance: $m = -s, -s+1, \cdots, s-1, s$. The coordinate system is in general arbitrary, but often the projection axis, called z-direction, is chosen parallel to an external magnetic field or any other globally distinctive direction.

Ladder operators are linear combinations of the spin components orthogonal to the z-direction. They alter the magnetic quantum number m by ± 1, where normalisation factors $\mathrm{N}^{\pm}$ occur:

$$\underset{\sim}{S}^{\pm} = \underset{\sim}{S}^x \pm \mathrm{i}\underset{\sim}{S}^y \tag{4.3}$$

$$\underset{\sim}{S}^{\pm}|s,m\rangle = \mathrm{N}^{\pm}(s,m)\,|s,m\pm 1\rangle \tag{4.4}$$

$$\mathrm{N}^{\pm}(s,m) = \hbar\sqrt{s(s+1) - m(m\pm 1)} \tag{4.5}$$

Spin systems often involve more than one spin. Usually product states

$$|m_1; m_2\rangle = |s_1, m_1; s_2, m_2\rangle = |s_1, m_1\rangle \otimes |s_2, m_2\rangle \tag{4.6}$$

are an obvious choice as a basis of the full Hilbert space. If all spins have identical s, the leftmost notation is used, otherwise the middle is preferred as a shorthand notation for the right hand side.

Spin operators obey the commutation relation

$$\left[\ \underset{\sim}{S}_k^{\alpha}\ ,\ \underset{\sim}{S}_l^{\beta}\ \right] \ = \ \mathrm{i}\,\hbar\ \delta_{kl}\ \varepsilon^{\alpha\,\beta\,\gamma}\ \underset{\sim}{S}_k^{\gamma}\ , \tag{4.7}$$

where the repeated index γ indicates a sum over the three spatial components of the spin vector. It can be rewritten as a cross product with itself:

$$\vec{\underset{\sim}{S}} \times \vec{\underset{\sim}{S}} = \mathrm{i}\hbar\vec{\underset{\sim}{S}}\ . \tag{4.8}$$

This is a reminder of the stark fact, that quantum operators are not to be confused with numerical values.

[1] This means systems consisting of an arbitrary number of identical spins interacting with each other via Heisenberg coupling of equal strength.

4.2. Spin Hamiltonian

In order to describe interactions of the spin system, it is modelled by a graph where nodes represent spins and edges between spin pairs represent interactions. Define $\mathcal{J}$ to be the set of edges (k,l) with non-zero interaction the full Hamiltonian of investigated systems can be written as

$$\underset{\sim}{H} = \sum_{(k,l)\in\mathcal{J}} \vec{\underset{\sim}{S}}_k \cdot \hat{J}_{k,l} \cdot \vec{\underset{\sim}{S}}_l \,, \tag{4.9}$$

where $\mathcal{J}$ contains all interacting pairs including $k = l$ and $\hat{J}_{kl}$ are 3-by-3 matrices containing interaction parameters. This is the most general form, if only terms consisting of products of at most two single-spin operators are allowed. The Hamiltonian should be hermitian, so we require $\underset{\sim}{H} = \underset{\sim}{H}^\dagger$. By comparison of coefficients we find that $\hat{J}_{kl} = \hat{J}_{kl}^*$ for $k \neq l$ and $\hat{J}_{kk} = \hat{J}_{kk}^\dagger$ are required.

So for $k \neq l$ interaction matrices need to be real-valued. These can be uniquely decomposed into a symmetric and an antisymmetric part. The antisymmetric part represents Dzyaloshinsky-Moriya interaction, whereas the symmetric part can be further decomposed into a diagonal matrix proportional to the identity matrix, which gives isotropic Heisenberg exchange. The remaining symmetric part is an anisotropic extension of the Heisenberg exchange. For $k = l$ the interaction matrix itself has to be hermitian. As real part of these we find single ion anisotropy terms, whereas the imaginary part can be identified as interaction with an external magnetic field using Equation 4.8.

4.2.1. Heisenberg Exchange

For isotropic Heisenberg Exchange the Hamiltonian can be written as

$$\underset{\sim}{H}_{\text{Heisenberg}} = -2 \sum_{(k,l)\in\mathcal{J}} J_{k,l}\, \vec{\underset{\sim}{S}}_k \cdot \vec{\underset{\sim}{S}}_l \,, \tag{4.10}$$

where $J_{k,l}$ is the interaction strength for spins k and l. Positive J-values correspond to ferromagnetic coupling, negative to antiferromagnetic coupling. With symmetric anisotropic exchange this can be extended to

$$\underset{\sim}{H}_{\text{Ani.Exch.}} = \sum_{(k,l)\in\mathcal{J}} \vec{\underset{\sim}{S}}_k \cdot \hat{J}_{k,l} \cdot \vec{\underset{\sim}{S}}_l \,. \tag{4.11}$$

4.2.2. Single Ion Anisotropy

Single ion anisotropy (SIA) is the influence of the spin's neighbourhood, e.g. symmetry of molecular coordination, bond type. As a second order term it can be written as

$$\underset{\sim}{H}_{\text{SIA}} = \sum_{k=1}^{N} \vec{\underset{\sim}{S}}_k \cdot \hat{D}_k \cdot \vec{\underset{\sim}{S}}_k = \sum_{k=1}^{N} \sum_{\alpha=x,y,z} D_\alpha \left(\vec{\underset{\sim}{S}}_k \cdot \vec{e}_k^{\,\alpha} \right)^2 . \tag{4.12}$$

The real valued, symmetric interaction matrices $\hat{D}_k$ can be diagonalised locally. The second equality uses their spectral decompositions to rewrite the SIA term. Usually a special form is found, which is for one ion in its local coordinate system

$$\underset{\sim}{H}_{\mathrm{SIA}} = D(\underset{\sim}{S}^z)^2 + E\left[(\underset{\sim}{S}^x)^2 - (\underset{\sim}{S}^y)^2\right] , D = \frac{3}{2}D_z , E = \frac{1}{2}(D_x - D_y) . \tag{4.13}$$

Here D and E are the (local) axial and rhombic zero field splitting (ZFS) parameters.

The axial anisotropy term is interesting for technical applications in data storage: A single metal ion with a large spin s, $E = 0$ and large $D < 0$ is a bi-stable system with energy barrier Ds^2 between the magnetic eigenstates with $m = \pm s$. Unfortunately real systems include terms that do not commute with $\underset{\sim}{S}^z$, thus allowing tunnelling processes between states $|s, \pm m\rangle$ which destroy the bi-stability of such systems.

4.2.3. Dzyaloshinsky-Moriya Interaction

This kind of antisymmetric exchange was first described by Dzyaloshinsky 1958, its relativistic origin – spin-orbit coupling – was found by Moriya 1960 [43, 44].

This contribution is strongest in systems with low symmetry, while high symmetry suppresses it. For a set $\mathcal{J}$ of ordered pairs of spins, the Dzyaloshinsky-Moriya interaction (DMI) can be written as

$$\underset{\sim}{H}_{\mathrm{DM}} = \sum_{(k,l)\in\mathcal{J}} \vec{a}_{k,l} \cdot \left(\vec{\underset{\sim}{S}}_k \times \vec{\underset{\sim}{S}}_l\right) , \tag{4.14}$$

where the vectors $\vec{a}_{k,l}$ denote interaction strength by their length while the directions are derived from spatial coordination by a given set of rules, often referred to as Moriya rules.

4.2.4. Zeeman

The Zeeman term describes interaction of spins with an external magnetic field $\vec{B}$:

$$\underset{\sim}{H}_{\mathrm{Zeeman}} = \mu_{\mathrm{B}} \vec{B} \cdot \sum_{k=1}^{N} \hat{g}_k \vec{\underset{\sim}{S}}_k , \tag{4.15}$$

where $\hat{g}_k$ is the Landé g-tensor of spin k and μ_{B} the Bohr magneton. Using Equation 4.8 the Zeeman term can be rewritten as in Equation 4.9.

Part III.

Results and Discussion

Festinare nocet, nocet et cunctatio saepe;
tempore quaeque suo qui facit, ille sapit.
– Ovid

5. Tests and Calibrations

In order to verify that the new algorithm works correctly, I revisit an example of a spin system where all observables can be calculated analytically. This allows for calibrating approximations via direct comparison of approximate and exact results.

5.1. Analytical Results: Spin Triangle

The spin triangle is an example of a system where identical spins in a Heisenberg model interact with each other with equal strength J – these systems are called pantaeder.

So the Hamiltonian is easily rewritten in terms of the total spin $\vec{\underset{\sim}{S}}_t$:

$$\underset{\sim}{H}_H = -2J \sum_{k<l} \vec{\underset{\sim}{S}}_k \cdot \vec{\underset{\sim}{S}}_l = -J \vec{\underset{\sim}{S}}_t^{\,2} + 3Js(s+1) \; . \tag{5.1}$$

$$\underset{\sim}{H}_Z = \mu_\mathrm{B} \vec{B} \cdot \sum_{k=1}^{3} g_k \vec{\underset{\sim}{S}}_k = g\mu_\mathrm{B} \vec{B} \cdot \vec{\underset{\sim}{S}}_t \; . \tag{5.2}$$

Defining the direction of the magnetic field as the z-direction, the total Hamiltonian of the triangle is

$$\underset{\sim}{H} = 3Js(s+1) - J \vec{\underset{\sim}{S}}_t^{\,2} + g\mu_\mathrm{B} B \underset{\sim}{S}_t^z \; . \tag{5.3}$$

The eigenvalues

$$\mathrm{E}\left(s, S_t, M_t\right) = \mathrm{E}\left(s, S_t, 0\right) + g\mu_\mathrm{B} M_t = 3Js(s+1) - JS_t(S_t+1) + g\mu_\mathrm{B} M_t \tag{5.4}$$

only depend on total spin quantum numbers $S_t \in \{s - \lfloor s \rfloor, \cdots, 3s-1, 3s\}$, where each value S_t occurs $\eta\left(S_t\right)$ times, and $M_t = -S_t, \cdots, S_t$. The algebraic multiplicity of total spin eigenvalues in a triangle is

$$\eta\left(S\right) = \begin{cases} 2S+1 & , \quad S \leq s \\ 3s+1-S & , \quad S \geq s \end{cases} \; . \tag{5.5}$$

This evaluation of total spin quantum numbers and multiplicities is easily extended to an arbitrary number N of identical spins, where

$$S_t \in \begin{cases} \left\{\frac{1}{2}, \cdots, Ns-1, Ns\right\} & , \quad \text{odd } N \text{ and half-integer } s \\ \{0, \cdots, Ns-1, Ns\} & , \quad \text{otherwise} \end{cases} \; . \tag{5.6}$$

So any pantaeder is a perfect model system for first tests, since all observables can be calculated analytically for any number N of identical spins with arbitrary quantum number s:

$$\mathrm{Z}(T,B) = \sum_{S_t} \eta(S_t) \sum_{M=-S_t}^{S_t} \exp\left(-\beta \mathrm{E}(s,S_t,M)\right) \tag{5.7}$$

$$\mathrm{M}(T,B) = \frac{g\mu_\mathrm{B}}{\mathrm{Z}(T,B)} \sum_{S_t} \eta(S_t) \sum_{M=-S_t}^{S_t} M \exp\left(-\beta \mathrm{E}(s,S_t,M)\right) \tag{5.8}$$

$$\left\langle\!\left\langle \underset{\sim}{H} \right\rangle\!\right\rangle(T,B) = \frac{1}{\mathrm{Z}(T,B)} \sum_{S_t} \eta(S_t) \sum_{M=-S_t}^{S_t} \mathrm{E}(s,S_t,M) \exp\left(-\beta \mathrm{E}(s,S_t,M)\right) . \tag{5.9}$$

In order to evaluate analytical results for the magnetisation, partial sums over magnetic quantum numbers in the partition function can be rewritten using Equation 5.4. With the Brillouin function

$$\mathrm{Br}_S(x) = \frac{2S+1}{2S}\coth\left((2S+1)x\right) - \frac{1}{2S}\coth(x) \ , x = \frac{g\mu_\mathrm{B}B}{2k_BT} \tag{5.10}$$

the magnetisation is

$$\mathrm{M}(T,B) = \frac{g\mu_\mathrm{B}}{\mathrm{Z}(T,B)} \sum_{S_t} \eta(S_t) \exp\left(-\beta E(s,S_t,0)\right) S\,\mathrm{Br}_{S_t}(x) . \tag{5.11}$$

These were used in first tests of the implemented routines:

- Rotations of the system, in order to have the external field direction as global z-direction and projection axis.
- General test of the Hamiltonian i. e. on-the-fly calculation of matrix elements in the matrix-vector multiplication routine, separately for each occurring term including SIA, DMI and Zeeman interaction.
- Test of difference quotients, see next section.

5.2. Difference Quotients

In order to find appropriate values of ΔB for calculation of difference quotients, here several values are tested. A spin triangle with $s = \frac{5}{2}$ is considered, where analytical results are compared to approximations. The Magnetisation plot shown in Figure 5.1 exhibits deviations not only for large values of ΔB, but also for small values, especially close to steps in the magnetisation. At the first plateau ($M = 11\,\mu_\mathrm{B}$) in the figure approximations with $\Delta B = 10^{-4}\,\mathrm{T}$ and $\Delta B = 10^{-5}\,\mathrm{T}$ overshoot before reaching the true value. At the second plateau ($M = 11\,\mu_\mathrm{B}$) at least $\Delta B = 10^{-5}\,\mathrm{T}$ yields a slightly too low value.

In Figure 5.2 the plot of specific heat data deviations are enhanced: Too large values of ΔB could even shift maxima and minima to positions of opposite extrema. Between $\Delta B = 0.50\,\mathrm{T}$ and $\Delta B = 0.10\,\mathrm{T}$ these shifts disappear and extrema are at correct positions. For smaller values of ΔB there is no obvious tendency, only the height of extrema varies.

Considering this, there is a window $0.10\,\mathrm{T} \geq \Delta B \geq 10^{-4}\,\mathrm{T}$ where acceptable approximations are to be expected. Larger values lead to obviously wrong results, lower values are inadvisable for numerical reasons.

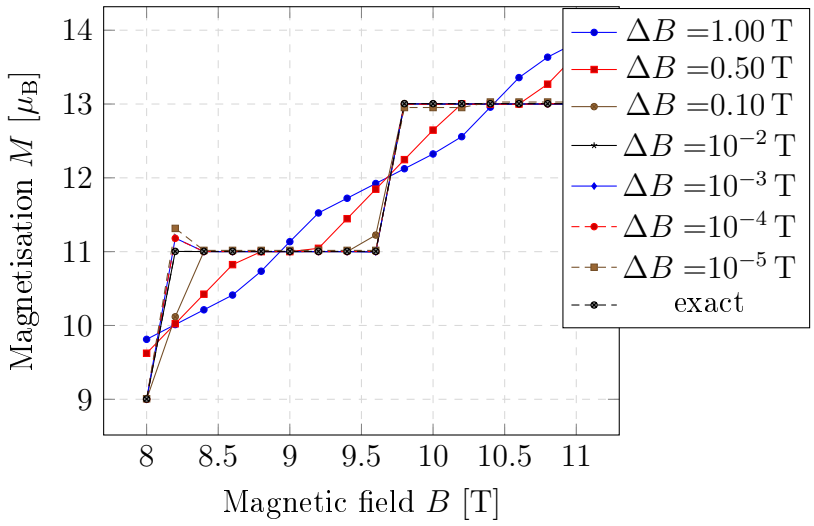

Figure 5.1.: Difference Quotient: Magnetisation
FTLM results implementing differential quotients with $\Delta B = 1.00\,\mathrm{T}$, $0.50\,\mathrm{T}$, $0.10\,\mathrm{T}$, $10^{-2}\,\mathrm{T}$, $10^{-3}\,\mathrm{T}$, $10^{-4}\,\mathrm{T}$ *and* $10^{-5}\,\mathrm{T}$ *at* $0.01\,\mathrm{K}$ *using* $R = 10$, $N_L = 40$ *compared to results of exact calculations.*

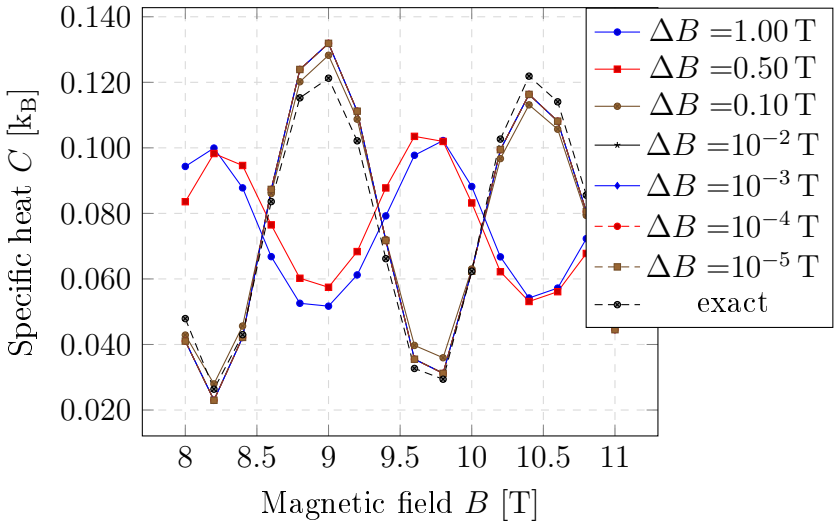

Figure 5.2.: Difference Quotient: Specific Heat
FTLM results implementing differential quotients with $\Delta B = 1.00\,\mathrm{T}$, $0.50\,\mathrm{T}$, $0.10\,\mathrm{T}$, $10^{-2}\,\mathrm{T}$, $10^{-3}\,\mathrm{T}$, $10^{-4}\,\mathrm{T}$ *and* $10^{-5}\,\mathrm{T}$ *at* $0.41\,\mathrm{K}$ *using* $R = 10$, $N_L = 40$ *compared to results of exact calculations.*

5.3. Drawbacks

One severe drawback emerged in FTLM calculations of the effective magnetic moment $\mu_{\text{eff.}}$ At high temperatures interactions are suppressed, so the system acts like a paramagnet. Therefore $\mu_{\text{eff.}}$ should approach a constant value, the paramagnetic limit. Consider the approximation to the thermodynamic expectation value of the magnetisation for infinite temperature, which is proportional to the trace of the total spin operator $\underset{\sim}{S}_t^z$:

$$M_\infty = \lim_{T\to\infty} \frac{g\mu_{\text{B}}}{Z} \text{Tr}[\underset{\sim}{S}_t^z \exp\left(-\beta \underset{\sim}{H}\right)] = \frac{g\mu_{\text{B}}}{\text{Dim}\left(\mathcal{H}\right)} \text{Tr}[\underset{\sim}{S}_t^z] = 0 \,. \tag{5.12}$$

In FTLM approximations this is unfortunately not zero, due to numerical instability. As a result the effective magnetic moment, which should reach a constant value for $T \to \infty$, tends to a line with slope M_∞ for positive values, whereas $\mu_{\text{eff.}}$ is singular for negative values.

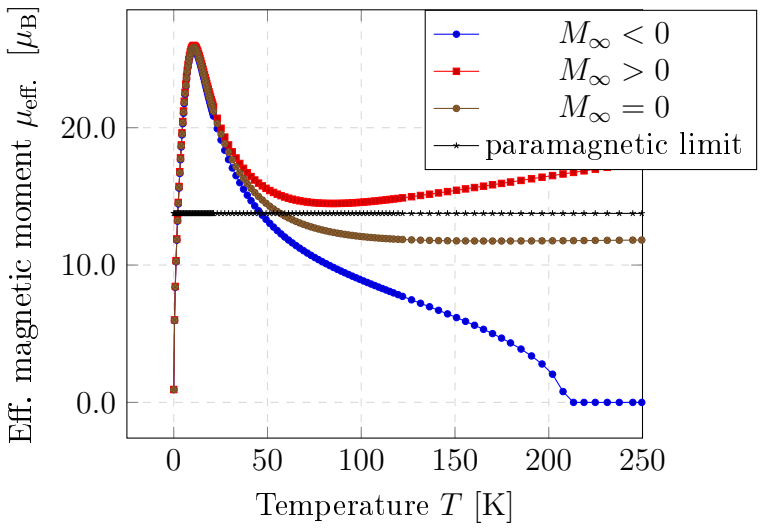

Figure 5.3.: Deviating asymptotics
Naive version results for $\mu_{\text{eff.}}$: Non-zero approximation of M_∞ results in deviating asymptotic behaviour; linear for positive, singular for negative values

To counteract this effect I had to improve the trace estimate. This was done by restoring a symmetry that helped before [45]:

$$\text{M}\left(T, -\vec{B}\right) = -\text{M}\left(T, \vec{B}\right) \,. \tag{5.13}$$

This was used to reduce the computational effort by a factor of two in case of preserved $\vec{S}_t^z$ quantum numbers. The contribution of Zeeman interaction could be evaluated after calculating approximate eigenvalues in a subspace with fixed quantum number M for both M and $-M$. In order to retain this effect I rebalanced full-space FTLM calculations by using symmetry partners of the starting vectors. Since for all calculations the $\vec{m}$-basis is used and the direction of the external magnetic field

is taken as global projection axis, it is easily achieved by reversing all magnetical quantum numbers. So for each starting vector $|\phi_r\rangle$ I created another vector:

$$\text{Given } |\phi_r\rangle = \sum_{\vec{m}} c_{\vec{m}} |\vec{m}\rangle \text{ , then take } |\phi'_r\rangle = \sum_{\vec{m}} c^*_{\vec{m}} |-\vec{m}\rangle \,. \tag{5.14}$$

Applying LP to the union of both sets improved results tremendously, while increasing computational effort only by a factor of two [46].

As stated before in my diploma thesis [45], one starting vector is sufficient to obtain good approximations. A larger number of starting vectors reduces statistical error estimates and averages out fluctuations. So one merely has to be careful about the number of steps to perform. If too few Lánczos steps are performed, magnetisation steps get suppressed, comparable to the effect of a higher temperature. Too many steps may result in tiny weight factors assigned to ground state energies and thus strong divergence of results close to zero temperature as well as magnetic field. Derived quantities calculated from expectation values such as $T\chi$ or $\mu_{\text{eff.}}$ suffer from inflation of these numerical errors close to zero true values.

6. Main Results

The results reviewed here have been published in [46] and [37]. In Section 6.1 two prototypes of Glaser's hourglass molecules are discussed, the first without central ion. The Mn_{12}–ring in Section 6.2 is the first case, where only FTLM results are present. After these Section 6.3 evaluates these first test cases of full Hilbert space calculations. Finally results for the famous Mn_{12} – acetate molecule are reviewed in Section 6.4.

6.1. Hourglass Molecules

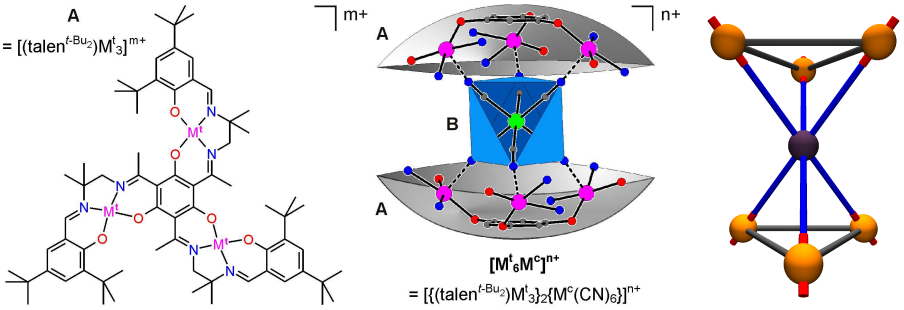

Figure 6.1.: Model and Structure of Hourglass Molecules
Left: Chemical structure of talen–caps [47].
Middle: Sketch of full structure [48, 49]. Triangle metal ions M^t (magenta) correspond to orange balls on the right. The central metal M^c (green) corresponds to the violet ball.
Right: Ball and stick model representing interactions and magnetic centres.

Figure 6.1 shows on the left a ball and stick model which is a schematic representation of the hourglass molecules investigated here. The symmetry of the model Hamiltonian rather than the molecular structure is shown.

Orange spheres represent manganese ions, the purple sphere represents the location of an additional central chromium ion. Lines (blue and grey) represent Heisenberg interactions. Red bars represent directions of easy axes, which are parallel to edges connecting manganese ions to the centre.

In the middle and on the right the chemical structure is represented: On the right a sketch of the full structure is shown, while the middle part of the figure shows the fixed structure of the top and bottom caps on the right. Metal ions and centre part remain unspecified, since there are several possible building blocks.

To find interesting molecules is quite easy. One class of molecule synthesised in Bielefeld are the hourglass-shaped molecules by Glaser's group [48, 49]. An example

is the Mn_6Cr molecule which consists of two C_3-symmetric triple-salen caps, each containing three Mn(III) ions ($s = 2$). The triangular caps are parallel to each other, but with a relative angle of 60°. The central building block is a Cr(IV) ion in octahedral coordination of cyanide ligands bridged via the nitrogen to Mn(III) ions of the caps. For all seven ions $g = 1.98$ is assumed.

This structure supposedly has a S_6-symmetry [48, 49] which suppresses E-term contributions of SIA. Thus less tunnelling processes are observed and the bi-stable ground states are expected to have a higher lifetime. Therefore this class of molecules is interesting for memory storage devices and effort is being made to coat surfaces of substrates with it [50].

Here I examine a model of the Mn_6Cr molecule and another version without the central Cr ion. On average the angle ϑ between global and local z-axes $\vec{e}_k^{\,z}$ (blue lines/red bars in Figure 6.1) typically has values near 40°[51], so we use $\vartheta = 40°$. For the central ion local and global coordinates coincide. It is assumed that the centre ion does not have SIA.

With this the Hamiltonian of the system is

$$\underset{\sim}{H} = J_\Delta(\underset{\sim}{\Delta}_{123} + \underset{\sim}{\Delta}_{456}) + J_\circ \underset{\sim}{\vec{S}}_7 \cdot \left(\underset{\sim}{\vec{S}}_\mathrm{t} - \underset{\sim}{\vec{S}}_7\right) + D\sum_1^6 (\underset{\sim}{\vec{S}}_k \cdot \vec{e}_k^{\,z})^2 + g\mu_\mathrm{B}\vec{B} \cdot \underset{\sim}{\vec{S}}_\mathrm{t} \ , \qquad (6.1)$$

where $\underset{\sim}{\vec{S}}_\mathrm{t}$ is the total spin operator and $\underset{\sim}{\Delta}_{abc} = \underset{\sim}{\vec{S}}_a \cdot \underset{\sim}{\vec{S}}_b + \underset{\sim}{\vec{S}}_b \cdot \underset{\sim}{\vec{S}}_c + \underset{\sim}{\vec{S}}_c \cdot \underset{\sim}{\vec{S}}_a$. The symbols J_Δ and $J_\circ$ denote Heisenberg coupling constants, the first couples ions in triangles, the second triangle-ions to the centre.

6.1.1. Fictive Mn_6 Molecule – Two Independent Triangles

As a first model system the hourglass molecule without central ion is examined. Without central ion the caps are isolated. In order to have C_3-symmetry in these triangles the coupling constants are set to a value of $J_\Delta = J = 0.314\,\mathrm{cm}^{-1}$. Easy axis anisotropy terms of equal strength of $D = 5.00\,\mathrm{cm}^{-1}$ are assumed along local z-directions which point outwards along the connections between the centre and each ion. One missing ingredient is the angle ϑ between the global and local z-axes, which we set to $\vartheta = 40°$. Without central ion surely $J_\circ = 0.00\,\mathrm{cm}^{-1}$ is a sound choice.

In the following influence of method parameters (number of steps and starting vectors) are examined. Figure 6.2 shows approximations of $\mu_\mathrm{eff.}$ for different values of R and N_L. Here the temperature dependence of $\mu_\mathrm{eff.}$ is simple: A steep ascent from zero to a maximum, after that a descent down to the paramagnetic limit. At very low values of N_L there is a wide temperature range where the approximation is far off. But increasing from $N_L = 4$ to $N_L = 8$ the approximation is much better.

In Figure 6.3 the effective magnetic moment versus temperature at $B = 1\,\mathrm{T}$ is shown. Blue lines correspond to ferromagnetic coupling while red lines corresponds to antiferromagnetic coupling. Full lines represent reference calculations from exact diagonalisation, which are compared to FTLM results represented by thick dashed lines.

The right part shows data for magnetic field in z-direction, which is an easy axis. Antiferromagnetic curves grow monotonously towards the paramagnetic limit. In

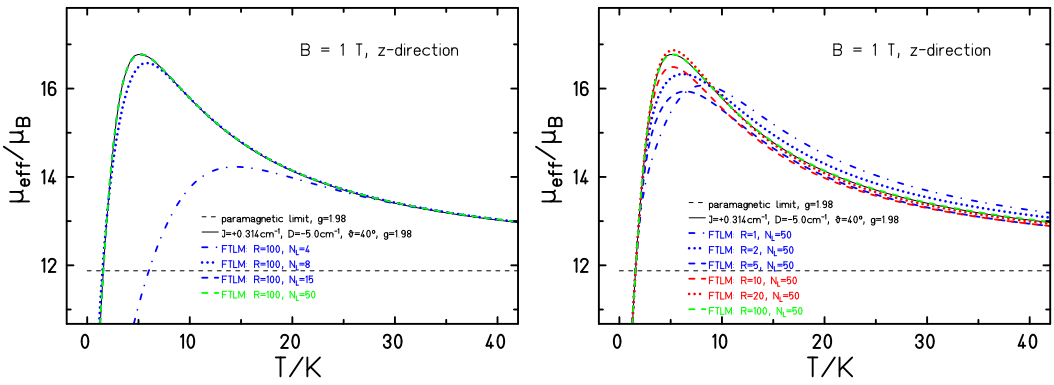

Figure 6.2.: Influence of R and N_L

FTLM results compared to ED. Left: The number of random vectors is fixed at $R = 100$ while the number of steps is varied. Right: The number of steps is fixed at $N_L = 50$ while the number of random vectors is varied [46].

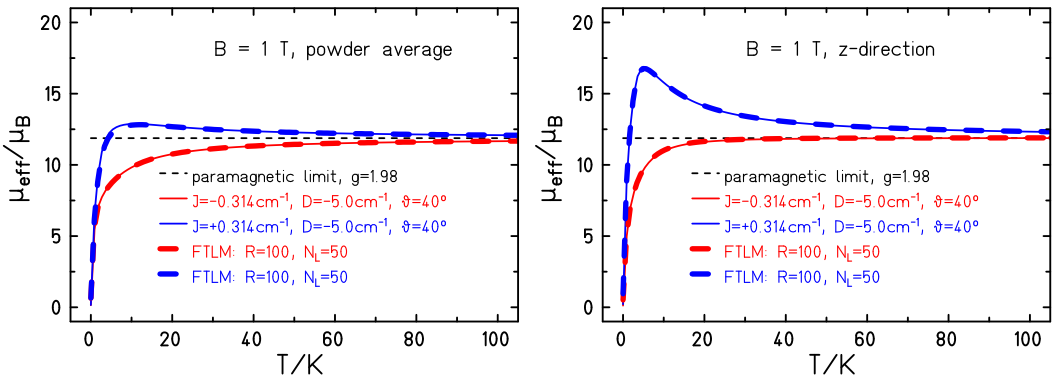

Figure 6.3.: Mn_6: $\mu_{\text{eff.}}$ vs. T

Full diagonalisation results as reference (full lines); FTLM results (thick dashed lines); Left: powder average; Right: z-direction; $B = 1\,\text{T}$. Red: antiferromagnetic; blue: ferromagnetic [46].

contrast to that, ferromagnetic curves exhibit a pronounced maximum far above the paramagnetic limit, then fall monotonously towards the limit.

On the left powder averaged data is shown. Antiferromagnetic curves take significantly longer to reach the limit, otherwise they look quite similar to single crystal data. However, for ferromagnetic data the maximum is changed significantly.

6.1.2. Fictive Molecule – Plus Central Ion

Now we add a central ion interacting at equal strength $J_\circ = J_2 = -6.00\,\mathrm{cm}^{-1}$ with each of the other ions. The absolute value of J_Δ remains and both signs are considered, so $|J_\Delta| = |J_1| = 0.314\,\mathrm{cm}^{-1}$. Easy axis anisotropy terms are not changed. These results show similar quality of approximation (for $R = 100, N_L = 50$) as before.

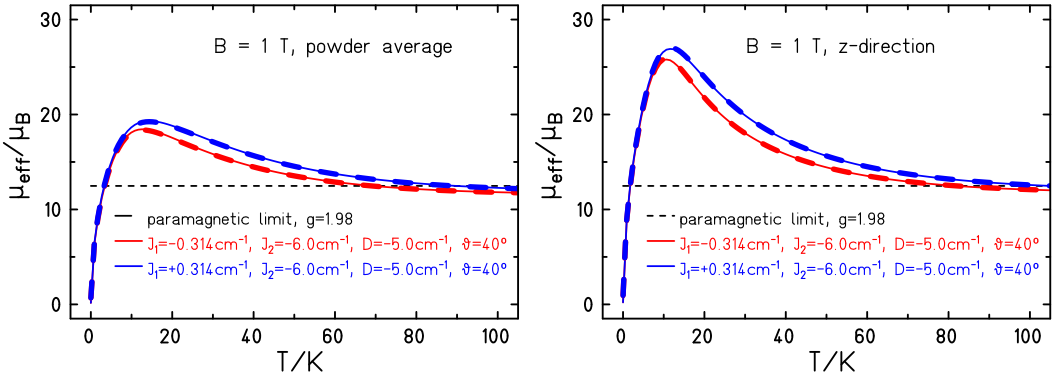

Figure 6.4.: Mn_6Cr: $\mu_{\mathrm{eff.}}$ vs. T
Full diagonalisation results as reference (full lines); FTLM results (thick dashed lines); Left: powder average; Right: z-direction; $B = 1\,\mathrm{T}$ [46]

6.2. Mn_{12}–Ring

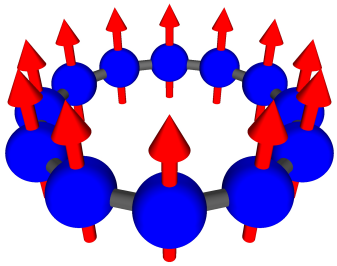

6.2.1. General Remarks

In order to study the feasibility of full Hilbert space FTLM calculations for spin systems with high-dimensional Hilbert space, we chose an anisotropic spin ring consisting of twelve Mn^{III} ions [46]. Given that $\underset{\sim}{S}^z$ is a conserved quantity i. e. only uni-axial D-tensor anisotropy is present and the magnetic field is applied parallel to the anisotropy axis, a symmetry-based partition of the Hilbert space allows for subspace calculations. Previously [52] we presented the symmetry-based FTLM and found good agreement of our approximations with exact calculations. These results are taken as reference for studying the quality of full-space FTLM.

The Hamiltonian of the system is

$$\underset{\sim}{H} = \sum_{k=1}^{12} J\vec{\underset{\sim}{S}}_k \cdot \vec{\underset{\sim}{S}}_{(k \bmod 12)+1} + D_k \underset{\sim}{S}_k^{z\,2} + g_k \mu_B \vec{B} \cdot \vec{\underset{\sim}{S}}_k \,, \tag{6.2}$$

where

$$D_k = D = -1.80\,\mathrm{cm}^{-1},\ |J| = 3.00\,\mathrm{cm}^{-1},\ g_k = g = 1.98.$$

For $s = 2$ the Hilbert space dimension $d = (2s+1)^{12} = 244\,140\,625$ is well beyond reach of ED. FTLM is necessary and no reference results are obtainable for magnetic field applied orthogonal to the anisotropy axis. So FTLM calculations performed leave previous limits far behind. Nevertheless, these calculations are quite time consuming, e. g. one data point calculated with $N_L = 50$, $R = 5$ took about eight hours on our local SMP machine.

6.2.2. Actual Results

The left part of Figure 6.5 shows calculated magnetisation data for both signs of the coupling constant J at $T = 2.00\,\mathrm{K}$. For positive sign the magnetisation reaches its saturation value already for quite small applied magnetic field in z-direction, so only one point is shown. The situation is different for the opposite sign: First the magnetisation remains (close to) zero, then near $B = 15.00\,\mathrm{T}$ it almost jumps to about $12\,\mu_B$. Then it grows linearly until it reaches its saturation value above 50 T.

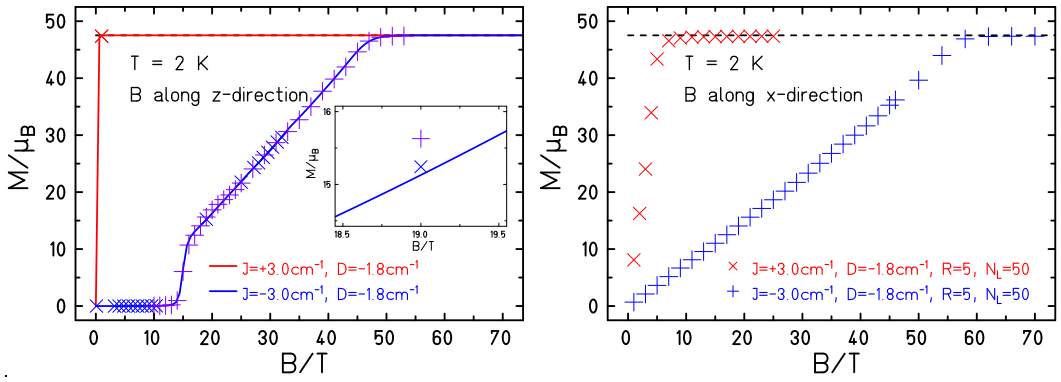

Figure 6.5.: Plot of Magnetisation data of a fictive Mn_{12}–ring at $T = 2.00\,\mathrm{K}$ *Left: z-direction; Right: x-direction; Inset: Comparison of FTLM results using* $R = 5$ *('+') and* $R = 50$ *('X'). Continuous lines display results of reference calculations [46].*

The inset in Figure 6.5 shows the resulting data points at $B = 19\,\mathrm{T}$ for $R = 5$ and $R = 50$ (times two for symmetry correction) starting vectors. For larger R the approximation approaches the reference value (solid line), thus confirming the expected behaviour of a Monte Carlo based process.

The right part presents "brand new" magnetisation data in the case of a magnetic field applied orthogonal to the anisotropy axis. The saturation is reached at field values that are about 10 T higher. For both signs of J it approaches the saturation value almost linearly, whereas features (plateau and jump) are obliterated.

For magnetic field in z-direction exact calculations were possible via decomposing the Hilbert space with respect to total $\underset{\sim}{S}^z$ quantum numbers. For magnetic field in x-direction this was no longer possible, because of the Zeeman term breaking conservation of the $\underset{\sim}{S}^Z$ quantum number. Full-space FTLM does not rely on the presence of (special) symmetries, calculations are still possible, without additional effort.

In Figure 6.6 approximate results for $\mu_{\mathrm{eff.}}$ vs. T in z-direction are shown. New approximations gained from full-space FTLM (thick, dashed lines) are compared to established reference results from the old, subspace based, FTLM (thin, continuous lines) both for ferromagnetic (red) and antiferromagnetic (blue) Heisenberg coupling. Calculations were done with $R = N_L = 50$ and agree almost perfectly.

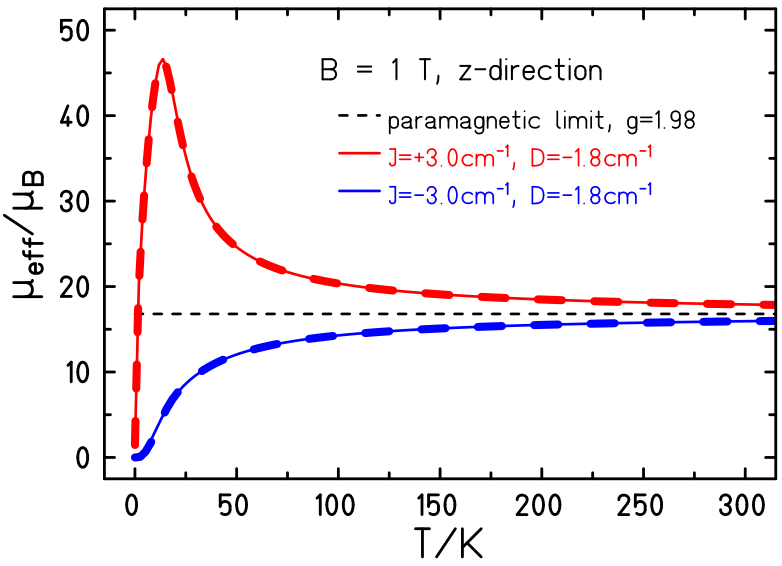

Figure 6.6.: Mn_{12}–ring: $\mu_{\text{eff.}}$ vs. T
Plot of effective magnetic moment versus temperature at $B = 1\,\mathrm{T}$ in z-direction with $R = N_L = 50$ [46]

6.3. Evaluation

After these first tests of FTLM for full Hilbert space calculations in this framework let us summarise what we expected of any calculated approximations and what was found.

Increasing the number of starting vectors R should have a stabilising effect i. e. Monte Carlo statistics apply. This means, that approximate values converge towards true values such that the error diminishes proportional to $\sqrt{R^{-1}}$. Looking at Figure 6.5 this seems confirmed.

Per construction FTLM should be correct for high temperatures and close to zero. The number of Lánczos steps N_L corresponds to a truncation of Taylor expansions of functions: After N_L steps a polynomial of degree less than N_L is evaluated numerically exact. Qualitatively one observes, that for lower temperatures or better resolution more steps are necessary, as seen in Figure 6.2.

Since FTLM relies heavily on weights generated in a Lánczos process, there might be systematic errors. As already seen in my diploma thesis [45], heat capacity or magnetic susceptibility at low temperatures as functions of magnetic field are most susceptible. Absolute values of peaks correspond to degeneracies of relevant eigenstates, so the weights could be observed here. As a result extrema and other features of these functions at "finite" temperature might show heavy fluctuation.

Powder averages involve more starting vectors so results should be more reliable. FTLM and ED results almost coincide for $R = 100$, $N_L = 50$ in Figures 6.3 and 6.4 as well as Figure 6.6 for $R = N_L = 50$. No difference of approximation quality is visible for z-direction and powder averaged results.

6.4. The Mn_{12} – acetate Molecule

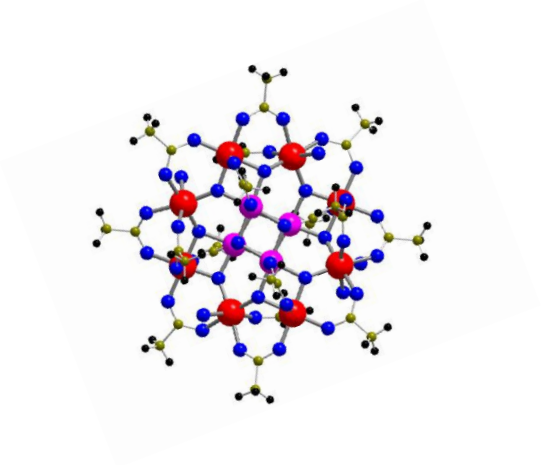

Figure 6.7.: The Mn_{12} – acetate molecule
Schematic representation of the Mn_{12} – acetate molecule [53].
red: Eight Mn(III) with $s = 2$,
magenta: Four Mn(IV) with $s = \frac{3}{2}$;
sum formula: $[Mn_{12}(CH_3COO)_{16}(H_2O)_4O_{12}] \cdot 2\,CH_3COOH \cdot 4\,H_2O$

6.4.1. General Remarks

The Mn_{12} – acetate SMM was synthesised almost forty years ago [16]. Several attempts were made to find a suitable description of the physical properties.

The magnetic centres of the Mn_{12} – acetate SMM are twelve manganese ions of two different valencies: Eight Mn(III) with $s = 2$ and four Mn(IV) with $s = \frac{3}{2}$, as illustrated in Figure 6.7. These compose a Hilbert space of dimension $d = 10^8$, which was too large for numerically exact calculations based on all eigenvalues of the full spin Hamiltonian. Instead large spin approximations were used i. e. the (total) ground state spin as well as effective anisotropy parameters were estimated to fit measured data.

Ab initio (DFT) calculations performed by Liechtenstein et al. [54] yielded a parameter set for a full spin Hamiltonian, which we used here.

In Figure 6.7 the chemical structure of Mn_{12} – acetate is shown. The magnetic centres i. e. manganese ions, are represented by red or magenta spheres while the rest determines and transfers interactions as well as anisotropy. A sketch of the model Hamiltonians structure as well as values of Heisenberg coupling constants are given in Figure 6.8.

Almost forty years after synthesis of Mn_{12} – acetate it is now possible to evaluate thermodynamic observables in a full spin Hilbert space framework. Thus parameter sets resulting from DFT or other calculations can now be put to the test by FTLM. This is done here, results for $\mu_{\text{eff.}}$ vs. T and M vs. B are presented in the following pages.

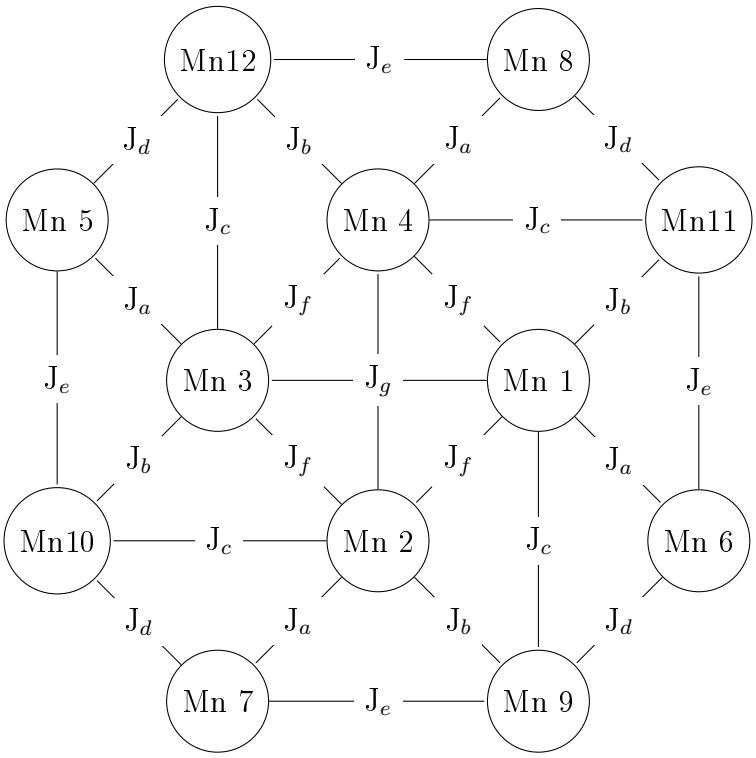

Table 6.1.: Coupling constants [meV]							
Ref.	J_a $(1,6)$	J_b $(1,11)$	J_c $(1,9)$	J_d $(6,9)$	J_e $(7,9)$	J_f $(1,4)$	J_g $(1,3)$
[53]	4.60	1.00	1.70	−0.50	−0.40	−1.60	−0.50
[54]	4.80	1.40	1.40	−0.50	−0.50	−1.60	−0.70
[55]	5.80	5.30	5.30	0.50	0.50	0.70	0.70
[56]	7.40	1.70	1.70	—	—	−2.00	—
[57]	10.30	10.20	10.20	2.00	2.00	−0.70	−0.70

Figure 6.8.: Coupling scheme of Mn_{12} −acetate
In this coupling scheme a C_4-symmetry is assumed (as in [53]), therefore coupling constants and SIA contributions are not arbitrary. The twelve magnetic centres are subdivided into three groups of four ions each. Members of each subgroup are related by symmetry transformations. The table lists a choice of different parameter sets proposed for this molecule.

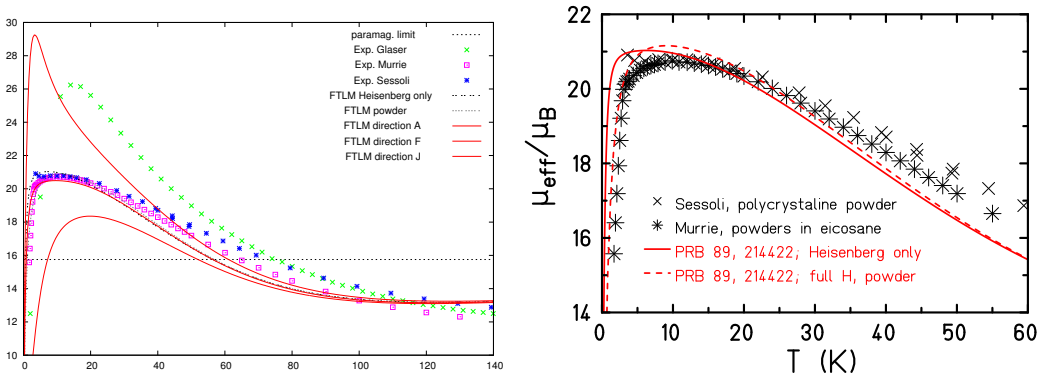

Figure 6.9.: Effective magnetic moment: Experiments vs. FTLM
On the left experimental data and approximate curves of the effective magnetic moment over temperature at $B = 0.13\,\mathrm{T}$ are shown. The directions are listed in Table 2.1. On the right measured data is compared to approximations for Heisenberg (full line) and full Hamiltonian (dashed line) [37].

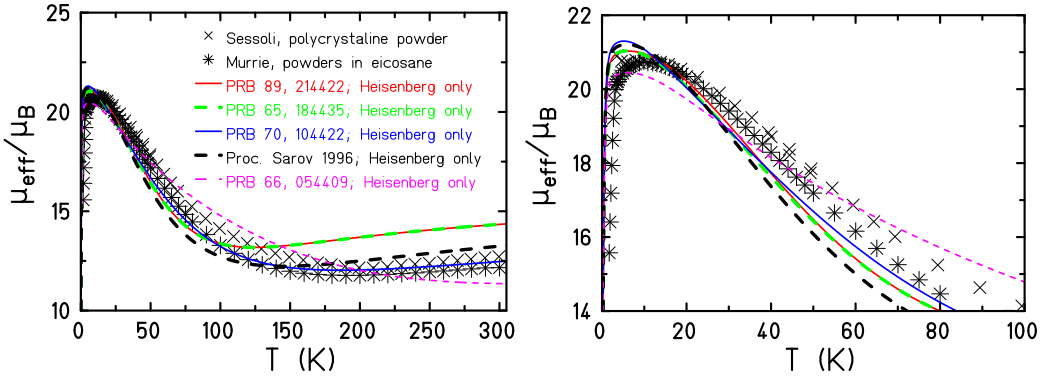

Figure 6.10.: $Mn_{12}-$acetate: $\mu_{\mathrm{eff.}}$; Heisenberg only
Measured data compared to theoretical results for different Heisenberg Hamiltonians. Right: Zoom [37]

6.4.2. Actual Results – $\mu_{\mathrm{eff.}}$ vs. T

In a recent publication [58] Tabrizi, Arbuznikov and Kaupp state correctly, that the coupling constants in our calculations are not the ones we intended to take, instead they differ by a factor of two from [53]. There are two reasons for this error to persist: A change of input encoding generated the undetected error, whilst the result was closer to the expected i. e. experimental data.

Analysis of data focuses on (effective) magnetization data. First consider the effect of anisotropy on the effective magnetic moment. In the left part of Figure 6.9 approximate curves for three directions of magnetic field are compared to experimental data. The paramagnetic limit is shown as a reference. Close to zero temperature all curves start below this value, cross at low temperatures and cross again. All data are below the paramagnetic limit at 80 K. Calculated curves almost coincide at 120 K and reach the paramagnetic limit from below at much larger temperature.

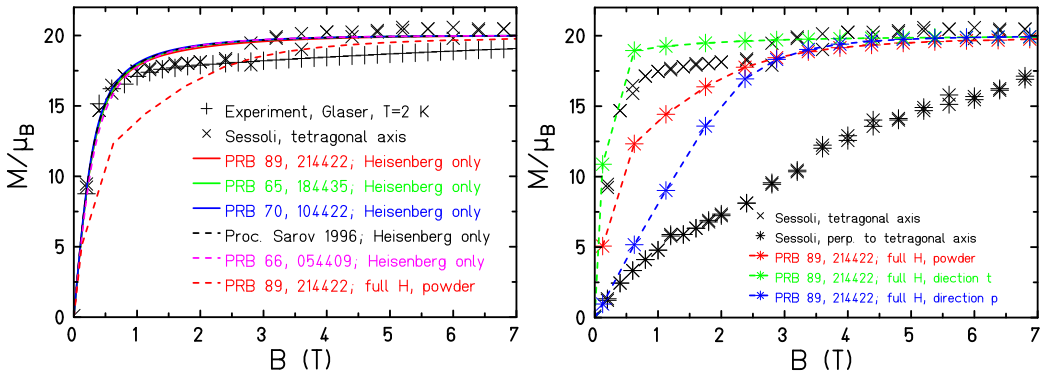

Figure 6.11.: Low field magnetisation data of Mn_{12} – acetate
Low field magnetisation data of Mn_{12} – acetate; Comparison of parametrisations to experiment; Left: Different parameter sets. Right: Chosen parameter set, different direction [37]

With increasing temperature anisotropy effects are suppressed first. Later every interaction is overcome by temperature, hence the paramagnetic limit is reached.

Experimental data measured by Glaser's group exhibit a behaviour similar to the curve corresponding to direction F (given in Table 2.1), which is close to the symmetry axis (z-direction) of the chosen parametrisation. This leads to the conclusion, that this data is taken from a single crystal or a loose powder that rearranged itself during measurement. The other two data sets coincide at low temperatures and seem to be taken from powder samples. In addition to this curves of the Hamiltonian without anisotropy as well as a powder average are shown.

The right part of Figure 6.9 shows these at low temperatures: The Heisenberg only curve reaches its maximum first, but its position is too low in temperature (the missing factor of two would move it even lower). For the powder average of the anisotropic model the maximum is shifted to higher temperatures. Its position is in good agreement with measured data, but its value is too high.

6.4.3. Actual Results – M vs. B

Next consider magnetisation as a function of the external field B.

In Figure 6.11 low field magnetisation data is shown. In the left part Glaser's experimental data as well as measurements along the symmetry axis done in Sessoli's group are compared to FTLM approximations using the Heisenberg only parameter sets listed in Table 6.1, see Figure 6.8. In the right part experimental data from Sessoli's group is compared to FTLM approximations. Experimental data is taken along the symmetry axis and one direction perpendicular to that. Approximations are taken perpendicular (direction p) and almost parallel (direction t) to the symmetry axis.[1] Powder averaged data is shown as well in both parts.

In the left part two experimental data sets are shown. Sessoli's measurements

[1] The directions used for powder averaging are listed in *Table 2.1*. Directions t and p are equal to directions F and J in that table.

exhibit a step-like feature at $B \approx 2.50\,\mathrm{T}$, which might be due to a reorientation of/within the sample or some other change in experimental setup. Up to this point it is in quite good agreement with Glaser's measurements, where magnetisation increases further with a very small slope. Heisenberg only calculations are almost on top of each other. They are quite featureless curves saturating at a value of $M = 20\,\mu_\mathrm{B}$ as expected for the $S = 10$ ground state. The powder averaged approximation increases much slower, catching up at $B \approx 3.00\,\mathrm{T}$.

Part IV.

Final Words

When you're finished changing,
you're finished.

– Benjamin Franklin
according to the WWW

7. Conclusions

Thirty to forty years after the synthesis of Mn_{12} – acetate calculating magnetic properties and thermodynamics based on a full spin Hamiltonian is possible now. Earlier tests as well as the results reviewed and presented here verify that FTLM is a reliable, though approximate, method for obtaining information on large magnetic molecules.

Foundations for this work were already laid in my diploma thesis. Systems were modelled by a Heisenberg Hamiltonian with Zeeman interaction, therefore a projection of the total spin onto the z-direction, which was chosen along the direction of the external magnetic field, was a conserved quantity and gave rise to a "good quantum number", allowing for decomposition of the Hilbert space into smaller subspaces. Thus computational effort was reduced by decreasing the relevant dimension for diagonalisation of the Hamiltonian. Subspaces corresponding to quantum numbers of equal absolute value but opposite sign were incorporated just by taking two copies of one and adding the Zeeman energies accordingly. As a hidden benefit, weights of states with opposite quantum number were evenly balanced with respect to the weight factors in the FTLM approximation. With this evaluation of approximate traces of spin operators was numerically stable. Only magnetic susceptibility and heat capacity were strongly influenced by relative weights near crossing fields due to the intrinsic problem of LP to reveal correct multiplicities of eigenvalues.

Promising results and performance of FTLM found in my diploma thesis gave rise to further investigate this method, aiming at anisotropic systems. These usually involve terms in the Hamiltonian, that do not commute with projections of the total spin. Thus the helpful symmetry is destroyed and full Hilbert space calculation is unavoidable. So the aim of this work is to implement and test FTLM for the use in the high performance computing environment at the Leibniz Supercomputing Centre (LRZ).

For ED memory consumption and computational complexity scale as d^2 and d^3 respectively. For LP and FTLM only one dimensional factor remains. Assuming large values of d, memory consumption for the two-vector algorithm is roughly $\lesssim 3d$, mainly two vectors plus collected data scaling as N_L^2. Computational effort scales as $4RN_L^2d$ for each different value and direction of the external magnetic field. For powder averages this involves ten or more directions, so for $R = N_L = 50$ the pre-factor is almost $50^4 = 62\,500$. Assuming equal proportionality, computational complexity and memory storage both are reduced by a factor of d. Taking $R = 100$ and $N_L = 120$ as ultima ratio one could argue, that FTLM beats ED at $d \sim 10^4$. With linear complexity and memory consumption FTLM extends the limits by several orders of magnitude.

Still FTLM works for large anisotropic systems, since computational effort and time consumption increase only linearly with the dimension. For the hour glass

molecules with a Hilbert space dimension of $d = 62\,500$ computations were still possible on a laptop PC, even for the Mn_{12} – acetate molecule with $d = 100\,000\,000$ two vectors fit into memory and calculations were possible, but time-consuming.

Since full dimensional matrix transformations and the required storage for keeping intermediate vectors would render FTLM ineffective, a different solution is used: In order to calculate approximations of observables a "natural" thermodynamic potential proportional to the logarithm of the partition function is defined and two-sided difference quotients approximate derivatives. This requires repeating LP for two values of external field, which only doubles computational effort.

First tests revealed a systematic numerical instability for calculation of $\mu_{\text{eff.}}$ So at first glance full dimensional matrix transformations would seem necessary. Fortunately, this is remedied by using for each starting vector also an inverted copy, thus rebalancing weights for calculation of approximate traces. With this computational effort is doubled to overcome the drawback whilst preserving the main advantage of LP and FTLM. Already confirmed results of ED and symmetry-based FTLM calculations are in good agreement with new full-space FTLM approximations, seemingly getting better with increasing Hilbert space dimension.

So by replacing exact diagonalisation by this approximate method, formerly impossible tasks in the field of molecular magnetism are finally within reach. As a proof of principle, calculations for the Mn_{12} – acetate obtained from a full spin Hamiltonian are done for the first time.

7.1. Future Work

- Here mainly qualitative observations on errors were done. It would be nice to have quantitative estimates as error bars. This requires a rigorous analysis of numerical errors and their propagation to final results.
- To increase the upper limit of reachable Hilbert space dimension, implementations of FTLM – with special consideration of the very sparse structure of model Hamiltonians – for MPI or on GPUs can help a lot.
- Since FTLM yields reliable results, investigation of further magnetic molecules and materials are to be expected.
- An extension to approximate nonequilibrium properties and correlation functions is already proposed and used, so it is only a small step to do so for spin systems, too.

Bibliography

[1] Sheikh, J.A.; Adhikary, A.; and Konar, S. (2014). *Magnetic refrigeration and slow magnetic relaxation in tetranuclear lanthanide cages (Ln = Gd, Dy) with in situ ligand transformation.* New J. Chem., 38(7):3006–3014.

[2] Liu, J.L.; Chen, Y.C.; Guo, F.S.; and Tong, M.L. (2014). *Recent advances in the design of magnetic molecules for use as cryogenic magnetic coolants.* Coord. Chem. Rev., 281:26–49.

[3] Tejada, J.; Chudnovsky, E.M.; del Barco, E.; Hernandez, J.M.; and Spiller, T.P. (2001). *Magnetic qubits as hardware for quantum computers.* Nanotechnology, 12(2):181.

[4] Wende, H. (2009). *Molecular magnets: How a nightmare turns into a vision.* Nat. Mater., 8(3):165–166.

[5] Mannini, M.; Pineider, F.; Sainctavit, P.; et al. (2009). *Magnetic memory of a single-molecule quantum magnet wired to a gold surface.* Nat. Mater., 8(3):194–197.

[6] Schollwöck, U. (2005). *The density-matrix renormalization group.* Rev. Mod. Phys., 77(1):259–315.

[7] Towler, M.D. (2006). *The quantum Monte Carlo method.* physica status solidi (b), 243(11):2573–2598.

[8] Lester Jr., W.A.; Mitas, L.; and Hammond, B. (2009). *Quantum Monte Carlo for atoms, molecules and solids.* Chem. Phys. Lett., 478(1–3):1–10.

[9] Troyer, M. and Wiese, U.J. (2005). *Computational Complexity and Fundamental Limitations to Fermionic Quantum Monte Carlo Simulations.* Phys. Rev. Lett., 94(17):170201.

[10] Lánczos, C. (1950). *An iteration method for the solution of the eigenvalue problem of linear differential and integral operators.* J. Res. Nat. Bur. Stand., 45:255–282.

[11] Lánczos, C. (1952). *Solution of systems of linearized equations by minimized iterations.* J. Res. Nat. Bur. Stand., 49:33–53.

[12] Golub, G.H. and Meurant, G. (1994). *Matrices, Moments and Quadrature.* In *NUMERICAL ANALYSIS*, pp. 105–156.

[13] Bai, Z.; Fahey, G.; and Golub, G. (1996). *Some large-scale matrix computation problems.* J. Comput. Appl. Math., 74(1–2):71–89.

[14] Golub, G.H. and Meurant, G. (1997). *Matrices, Moments and Quadrature II; How to compute the norm of the error in iterative methods.* BIT Numerical Mathematics, 37(3):687–705.

[15] Bai, Z.; Fahey, M.; Golub, G.; Menon, M.; and Richter, E. (1997). *Computing Partial Eigenvalue Sum in Electronic Structure Calculations.*

[16] Lis, T. (1980). *Preparation, structure, and magnetic properties of a dodecanuclear mixed-valence manganese carboxylate.* Acta Crystallographica Section B, 36(9):2042–2046.

[17] Paige, C.C. (1976). *Error Analysis of the Lánczos Algorithm for Tridiagonalizing a Symmetric Matrix.* Journal of the Institute of Mathematics and its Applications, 18(3):341–349.

[18] Cullum, J. and Willoughby, R.A. (1985). *Lánczos Algorithms for Large Symmetric Eigenvalue Computations, Volume 1: Theory.* Birkhäuser, Boston, MA, USA.

[19] Cullum, J. and Willoughby, R.A. (1985). *Lánczos Algorithms for Large Symmetric Eigenvalue Computations, Volume 2: Programs.* Birkhäuser, Boston, MA, USA.

[20] Simon, H.D. (1984). *Analysis of the symmetric Lánczos algorithm with reorthogonalization methods.* Linear Algebra Appl., 61:101–131.

[21] O'Leary, D.P. (1980). *The block conjugate gradient algorithm and related methods.* Linear Algebra Appl., 29:293–322.

[22] Cullum, J. (1978). *The simultaneous computation of a few of the algebraically largest and smallest eigenvalues of a large, sparse, symmetric matrix.* BIT Numerical Mathematics, 18(3):265–275.

[23] Calvetti, D.; Reichel, L.; and Sorensen, D.C. (1994). *An implicitly restarted Lánczos method for large symmetric eigenvalue problems.* Electron. Trans. Numer. Anal., 2(1):21.

[24] Wu, K. and Simon, H.D. (1998). *Thick-restart Lánczos method for symmetric eigenvalue problems.* In A. Ferreira; J. Rolim; H. Simon; and S.H. Teng (editors), *Solving Irregularly Structured Problems in Parallel*, pp. 43–55. Springer Berlin Heidelberg, Berlin, Heidelberg.

[25] Schnack, J. (WS 2007/2008). *Vorlesung: Theoretische Physik III.* Universität Bielefeld, Bielefeld.

[26] Nolting, W. (2005). *Statistische Physik*, vol. 6 of *Grundkurs theoretische Physik.* Springer, Berlin.

[27] Schwabl, F. (2006). *Statistische Mechanik.* Springer, Berlin [u.a.].

[28] Jaklič, J. and Prelovšek, P. (1994). *Lánczos method for the calculation of finite-temperature quantities in correlated systems.* Phys. Rev. B, 49(7):5065–5068.

[29] Lebedev, V.I. and Laikov, D.N. (1999). *A quadrature formula for the sphere of the 131st algebraic order of accuracy.* In *Doklady Mathematics*, vol. 59, pp. 477–481. MAIK Nauka/Interperiodica.

[30] Gatteschi, D.; Sessoli, R.; and Villain, J. (2006). *Molecular Nanomagnets.* Mesoscopic Physics and Nanotechnology. OUP Oxford.

[31] Lyubina, J. (2017). *Magnetocaloric materials for energy efficient cooling.* J. Phys. D: Appl. Phys., 50(5):053002.

[32] DiVincenzo, D.P. (2000). *The Physical Implementation of Quantum Computation.* Fortschr. Phys., 48(9–11):771–783.

[33] Aromi, G.; Aguila, D.; Gamez, P.; Luis, F.; and Roubeau, O. (2012). *Design of magnetic coordination complexes for quantum computing.* Chem. Soc. Rev., 41(2):537–546.

[34] Natterer, F.D.; Yang, K.; Paul, W.; et al. (2017). *Reading and writing single-atom magnets.* Nature, 543:226–228.

[35] Guo, F.S.; Day, B.M.; Chen, Y.C.; et al. (2017). *A Dysprosium Metallocene Single-Molecule Magnet Functioning at the Axial Limit.* Angew. Chem. Int. Ed., 56(38):11445–11449.

[36] Goodwin, C.A.P.; Ortu, F.; Reta, D.; Chilton, N.F.; and Mills, D.P. (2017). *Molecular magnetic hysteresis at* 60 *kelvin in dysprosocenium.* Nature, 548:439–442.

[37] Hanebaum, O. and Schnack, J. (2015). *Thermodynamic observables of* mn_{12}*-acetate calculated for the full spin Hamiltonian.* Phys. Rev. B, 92(6):064424.

[38] Nolting, W. (1986). *Quantentheorie des Magnetismus 1, Grundlagen*, vol. 1. Teubner, Stuttgart.

[39] Nolting, W. (1986). *Quantentheorie des Magnetismus 2, Modelle*, vol. 2. Teubner, Stuttgart.

[40] Blundell, S. (2006). *Magnetism in condensed matter.* Oxford master series in condensed matter physics. Oxford Univ. Press, Oxford.

[41] Gatteschi, D. and Sessoli, R. (2004). *Molecular nanomagnets: the first 10 years.* J. Magn. Magn. Mater., 272-276, Part 2(0):1030–1036. In Proceedings of the International Conference on Magnetism (ICM 2003).

[42] Boca, R. (1999). *Theoretical Foundations of Molecular Magnetism*, vol. 1 of *Current Methods in Inorganic Chemistry.* Elsevier, Amsterdam.

[43] Dzyaloshinsky, I. (1958). *A thermodynamic theory of "weak" ferromagnetism of antiferromagnetics.* J. Phys. Chem. Solids, 4(4):241–255.

[44] Moriya, T. (1960). *Anisotropic Superexchange Interaction and Weak Ferromagnetism.* Phys. Rev., 120(1):91–98.

[45] Wendland, O. (2010). *Anwendung der thermischen Lánczos-Methode für Quantenspinsysteme.* Master's thesis (Diplomarbeit), Universität Bielefeld.

[46] Hanebaum, O. and Schnack, J. (2014). *Advanced finite-temperature Lánczos method for anisotropic spin systems.* Eur. Phys. J. B, 87(9):194–200.

[47] Hoeke, V.; Gieb, K.; Muller, P.; et al. (2012). *Hysteresis in the ground and excited spin state up to* 10 T *of a* $[Mn_6^{III}Mn^{III}]^{3+}$ *triplesalen single-molecule magnet.* Chem. Sci., 3(9):2868–2882.

[48] Glaser, T. (2011). *Rational design of single-molecule magnets: a supramolecular approach.* Chem. Commun., 47:116–130.

[49] Glaser, T.; Heidemeier, M.; Krickemeyer, E.; et al. (2009). *Exchange Interactions and Zero-Field Splittings in C_3-Symmetric $Mn_6^{III}Fe^{III}$: Using Molecular Recognition for the Construction of a Series of High Spin Complexes Based on the Triplesalen Ligand.* Inorg. Chem., 48:607–620.

[50] Gryzia, A.; Predatsch, H.; Brechling, A.; et al. (2011). *Preparation of monolayers of $[Mn_6^{III}Cr^{III}]^{3+}$ single-molecule magnets on HOPG, mica and silicon surfaces and characterization by means of non-contact AFM.* Nanoscale Res. Lett., 6(1):486.

[51] Hoeke, V.; Heidemeier, M.; Krickemeyer, E.; et al. (2012). *Environmental Influence on the Single-Molecule Magnet Behavior of $[Mn_6^{III}Cr^{III}]^{3+}$: Molecular Symmetry versus Solid-State Effects.* Inorg. Chem., 51(20):10929–10954.

[52] Schnack, J. and Wendland, O. (2010). *Properties of highly frustrated magnetic molecules studied by the finite-temperature Lánczos method.* Eur. Phys. J. B, 78(4):535–541.

[53] Mazurenko, V.V.; Kvashnin, Y.O.; Jin, F.; et al. (2014). *First-principles modeling of magnetic excitations in* Mn_{12}. Phys. Rev. B, 89(21):214422.

[54] Boukhvalov, D.W.; Lichtenstein, A.I.; Dobrovitski, V.V.; et al. (2002). *Effect of local Coulomb interactions on the electronic structure and exchange interactions in* Mn_{12} *magnetic molecules.* Phys. Rev. B, 65(18):184435.

[55] Chaboussant, G.; Sieber, A.; Ochsenbein, S.; et al. (2004). *Exchange interactions and high-energy spin states in* mn_{12}*-acetate.* Phys. Rev. B, 70(10):104422.

[56] Barbara, B.; Gatteschi, D.; Mukhin, A.A.; et al. (1997). *Nano-scale ferrimagnet Mn12Ac in ultra-high magnetic field.* In *Proceedings of Seventh International Conference on Megagauss Magnetic Field Generation and Related Topics*, p. 853. Sarov, 1996.

[57] Regnault, N.; Jolicœur, T.; Sessoli, R.; Gatteschi, D.; and Verdaguer, M. (2002). *Exchange coupling in the magnetic molecular cluster* mn_{12}Ac. Phys. Rev. B, 66(5):054409.

[58] Ghassemi Tabrizi, S.; Arbuznikov, A.V.; and Kaupp, M. (2016). *Understanding Thermodynamic and Spectroscopic Properties of Tetragonal mn_{12} Single-Molecule Magnets from Combined Density Functional Theory/Spin-Hamiltonian Calculations.* J. Phys. Chem. A, 120(34):6864–6879.